Portland State Aerospace Society
Launch Vehicle 4 Airframe

Final Report - Spring 2021

Group 10
Catie Spivey, Jim Foley, Melissa McEntire, William Bleichner, Matthew Bradbury

Academic Advisor
Dr. Sung Yi

Industry Advisor
Andrew Greenberg

Sponsoring Company
Portland State Aerospace Society

June 3, 2021

Table of Contents

Team Members

Catie Spivey: Team Lead. CAD: coupling rings, arc clamps, launch lugs, racepipe clamps, thrust plate. CFD: fin optimization at maximum Mach number and maximum dynamic pressure. Project management and coordination with sponsor.
catiespivey@gmail.com

Jim Foley: CFD Lead, CAD Assembly Co-Lead, UTEAP Lead. CAD: Main assembly, nose cone, ERS module, and bulkheads. CFD: Nose cone shape optimization at maximum dynamic pressure. MDO and propulsion team coordination. Purchasing and grant coordination.
jfoleyengineer@gmail.com

Melissa McEntire: Isogrid Lead. CAD: LOX and IPA fuel tanks with isogrid pattern, tank end caps, contributed to passthrough module modeling techniques, presented on and coached CAD best practices in a collaborative setting. FEA: End cap pressure failure.

William Bleichner: CAD Assembly Co-Lead. CAD: Main assembly, composite modules, fins and fin assembly. Contributed to modeling isogrid end caps and passthrough indexing system. FEA: Fin assembly attachment validation at maximum dynamic pressure.
william.bleichner@gmail.com

Matthew Bradbury: FEA Lead. CAD: camera/passthrough/RCS modules, racepipes. FEA: arc clamps, isogrid tank modules, camera/passthrough modules, launch lugs, launch lug assembly.
matthewbbradbury@gmail.com

Executive Summary

Project Objective Statement

The objective of this capstone was to design a rocket airframe capable of 100 km flight to meet the requirements of the Portland State Aerospace Society (PSAS) for their Launch Vehicle (LV4) rocket to compete in the Base 11 Space Challenge.

Final Status of the Design Project

Our customer requirements for this project included extracting performance requirements from the multidisciplinary optimization program (MDO) [1] to inform a detailed design of the LV4 airframe and all of its components to ensure that it meets or exceeds these requirements. The subsystems that constitutes the airframe are:

- Nose cone
- Electro-mechanical recovery system (ERS)
- Reaction Control System (RCS)
- Camera Module
- Avionics Module
- Isogrid propellent tanks
- Engine Module and rocket fins
- Propulsion Passthrough Modules
- Coupling Rings, arc clamps, launch lugs, and pipe clamps
- Bulkheads and thrust plate
- Racepipes
- Internal components

The CAD assembly and its modules and components went through three design phases, V1, V2, and V3. Each version underwent a design review with our customer and changes were made according to the feedback received. Other changes were made between phases based on results from FEA or CFD analysis. Many modeled components of the LV4 airframe are close to their final design for the rocket. Other components have been modeled the best they can be with the current available information. Future Capstones will have to do more work on designing components such as the Electromechanical Recovery System (ERS), Reaction Control System (RCS), avionics, and any modules related to propulsion functions which were out of the scope of this project. Additional future work should be done in refining and completing additional FEA and other structural analysis/experimentation as well as CFD to determine center of pressure and to further optimize fin and nose cone shapes.

Key Performance Metrics

This project's key goals were to determine the scalability of Launch Vehicle 3.1 (LV3.1) to LV4, meet the performance requirements of the MDO, and to determine the feasibility of the use of isogrid propellent tanks. The scalability from a 6" to a 12" diameter rocket has been determined to be possible and has met the structural requirements. The isogrid tanks have also proven to be achievable as test tanks are currently being manufactured. However, the rocket is currently 3 feet shorter than initially required by the length to diameter ratio of 27.6:1. Additionally, the total mass of the rocket and propulsion systems is larger than expected and thus some constraints of the MDO fail. The sponsor is reconsidering the constraints as the MDO changes.

1. Client/Market Requirements

The main requirement for this capstone was to determine if the modular design of LV3.1 (11.7 ft long with a 6.7 in outer diameter (OD)) could scale up to the larger LV4 (27.6 ft long with a 12 in OD) (Fig. 1) while retaining its functionality and proposed capabilities outlined by the MDO. The customer requirements matrix lists the main requirements for the capstone and how they relate to each section of the airframe and are found in Appendix D. Along with being scalable from LV3.1, LV4 needs to be fueled using liquid oxygen (LOX) and isopropyl alcohol (IPA) instead of the solid rocket fuel used in LV3.1. This required the capstone to design and analyse isogrid fuel tanks and test their manufacturability.

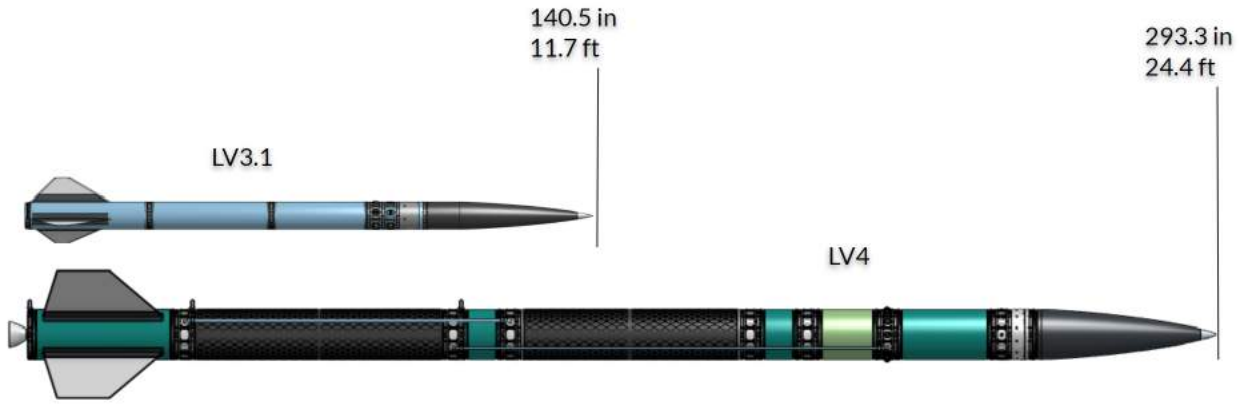

Figure 1: Size comparison of LV3.1 to LV4.

As the overall size of the rocket dramatically increased, our design process involved testing the form and capabilities of all rocket modules for structural integrity. This capability study was determined through a spiral design process (Fig. 2), by extracting theoretical numerical outputs from the LV4 MDO and using those results as a starting point with computer aided design (CAD), finite element analysis (FEA), and computational fluid dynamics (CFD) software programs to either validate and/or further refine the MDO. The total mass of the rocket was re-evaluated as constraints changed as the design progressed to verify if the theoretical calculations of the rocket reaching 93.21 ft/s at the launch rail, an overall dynamic pressure of 12.619 psi, and a maximum acceleration of 6.658 G's are feasible. The interdisciplinary nature of PSAS, including twice a week meetings with the sponsor, further contributed to the design spiral as we received constant feedback from other stakeholders such as other capstone teams and faculty advisors.

The CAD was first used to determine the feasibility of manufacturing, assembly, and storage of the modular airframe components. FEA was then used to determine the feasibility of the MDO structural requirements, including analysis of buckling, bending, and/or other failure modes, and to determine a design factor of safety. Finally, CFD was used to validate aerodynamic forces due to the high Mach number and dynamic pressures to be used in FEA.

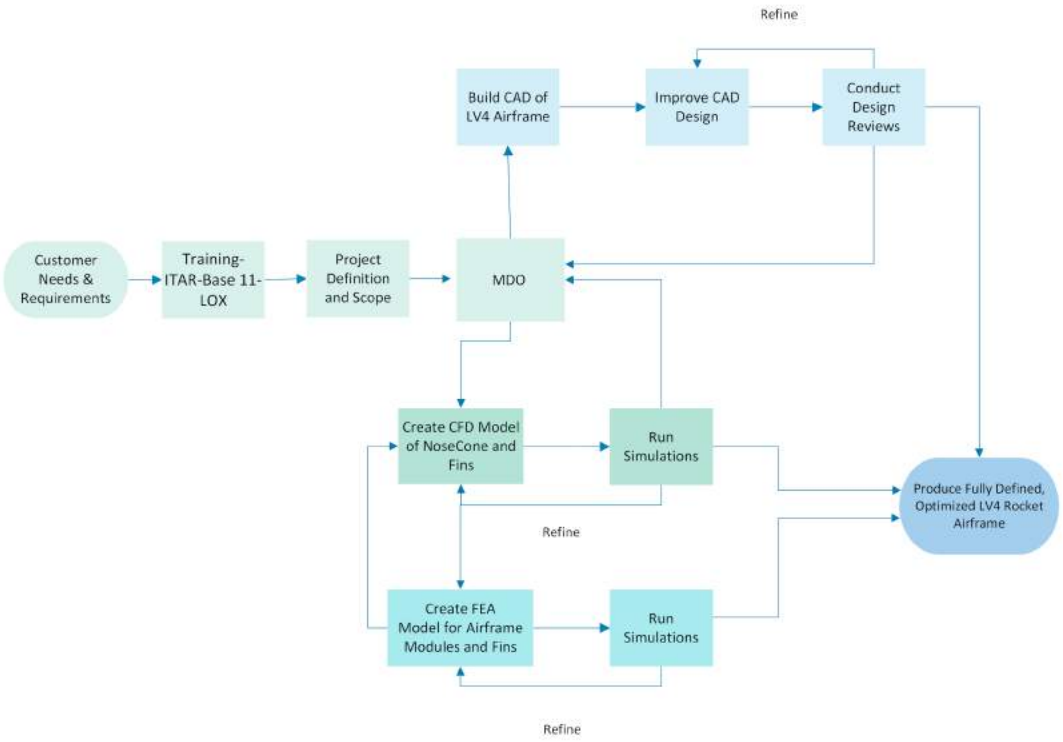

Figure 2: Project workflow detailing spiral design development process in use for the PSAS LV4 Airframe Capstone.

The final requirement for the team was to write the standard operating procedures for the design and manufacturing of all airframe components. This project must also be done under a Technology Control Plan (TCP) in order to meet the International Traffic in Arms Regulations (ITAR) restrictions that LV4 falls under.

2. Conceptual Design Summary

Entering the Base 11 Space Challenge has motivated PSAS to design a rocket capable of reaching a 100 km apogee using liquid fuel. In all previous versions of rockets designed by PSAS, the highest apogee reached was approximately 5.5 km. Previous rocket versions used commercial off the shelf (COTS) motors that utilized solid fuel. To design a rocket that uses liquid fuel and is capable of the 100 km apogee, a significant redesign of the previous rocket structure was needed. The latest rocket built by PSAS, LV3.1, provided the project of designing LV4 with an excellent starting point. The design of LV4 would take the airframe structure of LV3.1, which is a 6 in. diameter rocket, and scale it up to 12 in. diameter.

Before work began on the project, Base 11 required the team to undergo two different training courses, Base 11 Safety Training and NASA Liquid Oxygen (LOX) Safety Training. The team also attended an isogrid workshop hosted by a PSAS industry advisor, Peter McCloud (Appendix C.4). A failure modes and effects risk analysis on the system was also required (Appendix C.5).

When training was complete, the team began assessing the modules in LV3.1 CAD to determine the feasibility of scaling up the modules. Some subsystems were easier to scale up than others, some systems were unproven in previous rocket designs, and some systems did not exist and were new technologies for LV4. Modules such as the ERS, and passthrough modules were able to be scaled up with minor feature changes to accommodate the larger diameter rocket. The passthrough modules, which allow for internal components to pass between systems. now utilize a design that is modular and modifiable for additional use as the RCS and camera systems.

The composite modules will be made using a ⅛" Nomex sheet sandwiched between two layers of prepreg carbon fiber using an aluminum mandrel. The ends of each composite module, including the nose cone and engine module, will have coupling rings embedded for attachment to the next module. This process is the same as the LV3 layup process.

The avionics module will be the only composite module that uses fiberglass instead of carbon fiber in its construction. This is done because carbon fiber will cause interference with radio waves from the avionics system.

The isogrid propellant tanks are a new technology for PSAS and required significant attention to design. The isogrid workshop given by McCloud demonstrated the uses and benefits of isogrids and provided resources for determining feature sizes and strength, including the NASA isogrid design handbook [2]. For this project, the tanks are modeled using 6061-T6 Aluminum. Although not a requirement for this project, McCloud Aero is currently producing isogrid test tanks using funds from the Oregon Space Grant Consortium, Cooperative Agreement 80NSSC20M0035. The knowledge gained from the production of the test tanks helped inform the design for this project. FEA analysis was also done on the isogrid tanks end caps, which are welded on the tanks and designed to hold the pressure needed by the propulsion system. Unfortunately, OnShape, the CAD program used by the team, did not handle the rendering of the model well due to the computational load of the feature used to create the pattern, so the isogrid tanks had to be modeled in Solidworks.

The passthrough modules are also designed to be made out of 6061-T6 aluminum and can be used to serve several purposes. The passthroughs utilize a window design with 3D printed covers that can be customized for each subsystem such as cameras, race pipe interfaces, and any other propulsion needs. The passthrough modules also utilize an indexing system to assist with physical orientation during assembly of the rocket.

The nose cone and fins underwent CFD analysis to determine the optimal shapes. The nose cone compared two shapes to identify the best curve, also known as an ogive, in the supersonic regime. The fins compared four fin shapes and used the results from the CFD simulation to perform FEA to analyze the performance under pressure loading from the rocket in flight, looking at fin flutter and potential bracket delamination.

Each version of CAD for the individual modules and components requires a new version of a completed CAD assembly. For each iteration, design reviews were conducted with the sponsor/PSAS team and recommendations were brought back to the Capstone team to be implemented in the next design cycle. The final CAD assembly contained all of the modules and internal components (Fig. 3). This assembly required a significant amount of CAD mating work

to align the rocket in an orientation that matches the physical orientation. The front plane of the assembly matched what will be considered the front of the rocket, indicated by the indexing on the passthrough modules. Coupling rings and metal modules also have indexing arrows to indicate the joint placement between two arc clamps to ensure the launch lugs are aligned on the back of the rocket and allow racepipe clamps to be orientated by their respective windows in the passthrough modules. The racepipes were also added to the final assembly and their location was dictated by the needs of the propulsion team. These locations will be subject to change in later versions of the rocket as both future propulsion and the airframe teams continue to iterate the design.

The final assembly is then analyzed for its mass properties and these values are given to the MDO team. The MDO is then updated to produce expected flight parameters including speeds, apogee altitude, and thrust. Currently the MDO shows the rocket falling short of the target 100 km and further work will need to be done to reduce mass and optimize the rocket's design unless these constraints are changed by the sponsor, a decision currently under review.

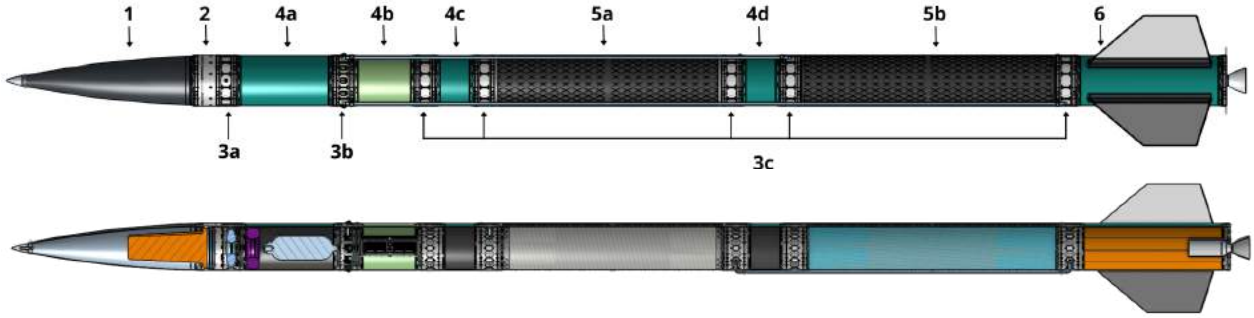

Figure 3 TOP: Version 3 of LV4 with subsystems labeled for Section 3. BOTTOM: Section view of LV4.

3. Subsystem Highlights

Figure 3 references the different subsystems/subassemblies of the LV4 airframe, with detailed images shown in Appendix A and design progress shown in Appendix C.1:

1: Nose Cone

The nose cone is a carbon fiber module. The nose cone shape of LV3.1 utilizes a Von Karman ogive. Research was done to understand why this shape was used over other types of nose cone shapes. The Von Karman ogive is an equation driven curve (Eq. 1,2) specifically developed to be effective at reducing drag [3]. This ogive can be further optimized by adjusting the fineness ratio, which is the ratio of the nose cone length to its diameter at the base of the curve. Using the equation for the Von Karman ogive and a given length from an earlier version of the MDO, the CAD was parameterized to build the model. The 6061-T6 Aluminum tip serves three functions: it helps diffuse heat build up at the tip, provides physical protection for the nose cone, and eases manufacturability of the nose cone due to the difficulty of creating a tip with carbon fiber.

$$\theta = arccos\left(1 - \left(2x/L_0\right)\right) \quad (1)$$

$$r = R/\sqrt{\pi}\sqrt{\theta - (sin(2\theta)/2)} \quad (2)$$

The nose cone also underwent CFD simulations (see Section 4) to compare the current version as a base case to another version with a 5:1 fineness ratio [4]. These simulations suggested that the base case shape with a fineness ratio of 3.6:1 was sufficient for the purpose of this project [Appendix C]. This was determined due to the significant amount of mass that would be added to the rocket to achieve a fineness ratio of 5:1, which is considered the best shape for maximum drag reduction.

2: ERS

The Electromechanical Recovery System (ERS) module was scaled up from LV3.1 and did not need many changes to accommodate the scaling. The current model is a two piece 6061-T6 Aluminum module held together by a twist coupling ring that activates when the rocket reaches apogee.

3: Passthroughs

The Passthrough modules are machined from 6061-T6 Aluminum and provide space for internal components such as wires and piping to travel between modules. The design was based on the LV3.1 camera module and scaled up to include 9 windows with the windows copying the same, proven design. The window covers have also been scaled up, with different modifications to allow for the different types of components that are attached to or pass through the windows. For the final version of these modules, 12 columns of countersunk through holes were added in between each window instance to allow for the easy attachment of bulkheads to the interior walls of the module, a design copied from LV3.1. The numbers found above each window outlet on the passthroughs were added as a final touch to aid in assembly and to help give a designation to the bookkeeping of where components will be housed. The odd numbered windows are lined up on center with the arc clamps (and thus these windows constrain the locations of the racepipes) and engraved arrows on the passthrough modules will designate the position of the end of the arc clamps placement.

a. RCS Passthrough

The Reaction Control System (RCS) module houses compressed nitrogen gas nozzles in three windows to allow for corrective in-flight alterations should the rocket experience any roll, pitch, or yaw deviations. The space in between these modules also allow for the passing through of wires, plumbing from the nitrogen tank, and other internals. The passthrough itself will connect to the ERS metal module on the top and the N2 composite module on the bottom by utilizing the coupling rings and arc clamps.

b. Camera Module

This aluminum passthrough module is the housing for nine onboard cameras and allows for the window covers to be used to access and manage internal onboard components. The camera passthrough will be joined to the N2 module at the top and the Avionics module on the bottom by way of arc clamps and coupling rings.

c. General Passthrough

The general pass through modules allow for the same passing through of components from exterior to interior and vice versa and will be updated with needs of the propulsion team.

4: Modules

a. Nitrogen Module

The N2 module is a carbon fiber composite module that will house a COTS pressurized nitrogen tank, which will operate the RCS and pressurize the IPA and LOX tanks. The composite modules consist of a layered sandwich of carbon fiber and Nomex honeycomb structure that are bonded to coupling rings. As decisions are made to add/exclude certain design features, the overall length of the composite modules may change within the constraints of the MDO. However, the composite modules will have to be cured in an oven and thus a maximum size restriction must be adhered to due to the size of the curing oven available to us.

b. Avionics Module

The avionics module is a composite module that houses the flight computer and communication systems. In lieu of carbon fiber, fiberglass is used because the carbon fiber material interrupts communication signals.

c. IPA Plumbing

The IPA Plumbing Module is a composite module that will house the isopropyl alcohol plumbing and delivery systems.

d. LOX Plumbing

The LOX Plumbing Module is a composite module that will house the liquid oxygen plumbing and delivery systems.

e. Fin Module

The composite fin module, colloquially known as the Fin Can, is a carbon fiber composite module with bonded carbon fiber brackets connecting the fins to its exterior.

5: Isotanks

a. Isotanks

The isotanks are 6061-T6 Aluminum modules which house isopropyl alcohol and liquid oxygen. The isogrid pattern is machined onto the outside of the aluminum cylinder. The isogrid pattern significantly reduces the weight of the tanks without sacrificing strength. These modules are modeled in FEA using a solid cylinder of an equivalent thickness. The pattern was determined by calculations done by McCloud [5].

b. End caps

The end caps are flat round plates that are welded into the ends of the isotanks. The decision to use flat end caps as opposed to hemispherical end caps was due to the inability to utilize friction-stir welding as a manufacturing process (usually needed for hemispherical pressure vessel end caps). Each end cap has an isogrid pattern machined into the outer surface of the cap. The end caps were added in V2 with a thickness of 0.25 in. After modeling in FEA (see Section 4 and Appendix G), the end caps were re-evaluated and changed to a thickness of 0.4 in.

6: Fins

Four fins will be machined out of 6061-T6 Aluminum and attached to the fin can with carbon fiber brackets. Several fin designs were examined for LV4. The final design is a trapezoidal planar geometry with a diamond-shaped cross section. The design was the best balance of key performance metrics such as minimal drag, suitable surface area, and minimized risk of damage during recovery. Data obtained from CFD and FEA were instrumental in validation of the current design (see Section 4 and Appendix E).

7: Racepipes

The racepipes allow for the flow of the compressed Nitrogen gas, Isopropyl Alcohol, and Liquid Oxygen down along the exterior of the rocket body, necessary due to the stacked design of the rocket tanks and the lack of internal space to house them inside of the rocket body. These are attached to the rocket through the odd numbered windows in the Passthrough modules and connect to their respective propulsion components. The location of the racepipes were constrained by the alignment of the racepipe clamps (mentioned in Coupling Rings and Arc Clamps) and windows and the needs of the Propulsion Team. The diameters, lengths, and materials of the racepipes were also dictated by the Propulsion Team.

8: Coupling Rings and Arc Clamps

The rocket is modular with each module connected via coupling rings and arc clamps, a technology that will be tested on LV3.1, machined from 6061-T6 Aluminum. The composite fiber modules are laid up onto the coupling rings (using the composite fiber "sandwich") while the aluminum modules have coupling rings machined into them. Six arc clamps join the rings together via 8 fasteners each and use a chamfer as a wedge to create a compressive preload on the rings to prevent shearing of the fasteners.

a. Launch Lugs

The launch lugs are used to hold the rocket on the launch rail and will be built into a modified arc clamp. This reduces the weight and height that would be needed to accommodate extra modules and allows for launch lugs to be placed between any modules. The size and shape of the bracket is determined by the requirements of the Base11 launch rail manufacturer.

b. Racepipe Clamps

Racepipe clamps were created for V3 in order to clamp the racepipes close to the body of the rocket, as requested by the sponsor. They are a modified version of the arc clamps that include a second clamp "top" that is fastened to the arc clamp "bottom" with four fasteners. Two strips of rubber padding are epoxied in place to dampen vibrations of the pipes inside the clamps. Two different diameters of clamps were created for the two different diameters of pipes. These clamps are not intended for structural support, only locational constraint, and thus do not need to undergo FEA or other stress analysis.

9: Miscellaneous

a. Bulkheads

Bulkheads are used to provide internal structural support for components in the passthroughs. Multiple iterations were part of the bulkhead design process to help mitigate mass in each successive model while maintaining a robust enough design for structural requirements.

b. Thrust Plate

An initial thrust plate was created for V3 based on the LV3.1 thrust plate. It acts as the bottom-most coupling ring to allow for placement of the bottom-most launch lug. Modifications were made to extrude the outer wall to provide more volume for the fasteners to thread into.

c. Internal RCS

Placeholder compressed Nitrogen gas nozzles were incorporated into our design phase V3 in order to give some representative mass and volume allowance for the RCS subsystem that is to be designed at a later date.

d. Internal ERS

The two piece ERS modules in LV3.1 are held together by a twist coupling that is turned by a motor to allow the two modules to separate at apogee to release the recovery parachute. In LV4 a simulated twist coupling was created with a cone-shaped mass to simulate the mass and volume of LV4's recovery system. The recovery system for LV4 will be designed by future teams and the modeled placeholder will eventually be replaced with a recovery system that will work with a 100 km rocket.

e. *Internal N2*

The Nitrogen tank module has a CAD model of a composite pressure vessel inside to simulate the mass and volume. The size and shape of this module will likely change according to the parameters developed by the propulsion teams.

f. Cubesat and Cradle

A 3U CubeSat, which will be used as the on-board avionics system, was integrated into the avionics module. An initial cradle to attach the CubeSat to the upper and lower bulkheads was also created. This cradle will need to be refined/improved on in the future.

g. IPA and LOX

The IPA and LOX were modeled as simple cylinders for mass representations in the assembly in V3.

h. Engine

A simple representation of the engine combustion chamber and exhaust nozzle is used to visually represent the engine placement and provide an initial mass estimate.

4. Performance Summary

<u>CFD</u>

Initial simplified CFD analysis on the nose cone and fins was completed in Star-CCM+ as part of the V2 phase in concordance with the final projects for our CFD class and further refined for the V3 phase. The focus was on drag and lift forces as well as location and magnitude of maximum pressure. This information was used to determine the best shapes of the nose cone and fin designs and, for the fins, contribute to the FEA models.

1. *Nose cone*

To prepare the nose cone for CFD a model was made in SolidWorks to simulate a wind tunnel and then imported into Star CCM+ for analysis. The analysis done was the expected boundary conditions when the rocket is at maximum dynamic pressure (Max Q). The conditions meant simulation was in the supersonic regime, with the rocket traveling at 699.5 m/s, or Mach 2.348, and experiencing an atmospheric pressure of 22,547 Pa. To simulate the aerodynamic flow in the supersonic regime, the solvers in Star CCM+ needed to be carefully chosen. The most important solver for this simulation was the Spalart-Allmaras Turbulence model [6]. The other features are shown in Appendix C.2 for reference. The nose cone with a fineness ratio of 3.6:1 was examined as the base case. This simulation produced drag coefficient results 0.42, which were expected based on previous research (Fig. 4).

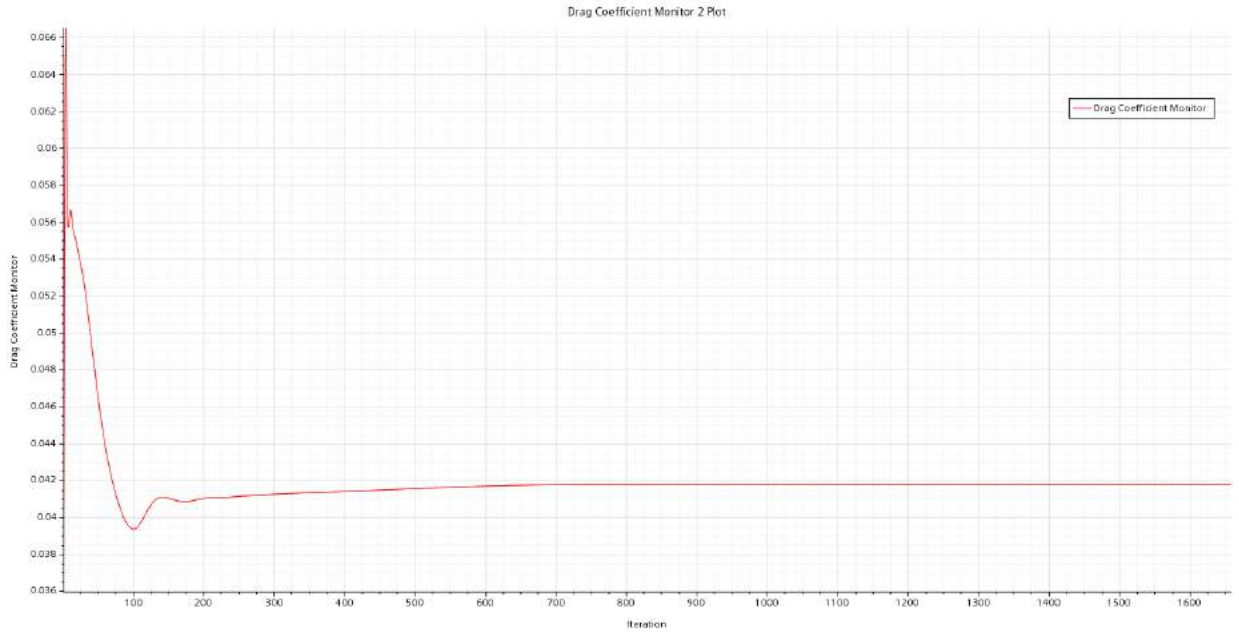

Figure 4: Drag Coefficient converging at approximately 0.042 for the base case nose cone.

To determine if the fineness ratio of 3.6:1 was sufficient, another simulation was done for a nose cone with a fineness ratio of 5:1, which is considered the upper limit of drag savings for the Von Karman ogive. The result did show drag savings compared to the 3.6:1 ratio but the simulated mass gain showed the improvements did not warrant a redesign of the nose cone shape (Table C.2.3).

2. *Fins*

For the V2 phase four different fin shapes were compared for the rocket traveling at maximum Mach number and the results of drag force and maximum pressure on the front of the fin were then used in FEA models to determine the likelihood of fin delamination (see FEA section). The V3 phase included refinement of the models and further analysis of the rocket traveling at maximum dynamic pressure. The diamond trapezoidal shaped fin was found to have the lowest drag force and lowest maximum pressure on the front surface. This shape of fin is also less likely to break upon landing compared to a swept fin (Appendix C.2 and E).

FEA

1. *Fins*

The fins of LV4 are fastened to the rocket fuselage via a bonded bracket. This design is based on the LV3.1 rocket. CFD simulations were performed based on the dimensions of the fin design and expected flight parameters of LV4 to determine the expected drag forces. With these values, FEA performed with theAbaqus/CAE program was used to validate this method of fin attachment for LV4. Two methods were used for this analysis, a composite shell model and a solid model. The shell model was selected because of the composite laminae feature, allowing the actual composite lay-up to be modeled. A solid model of the fin assembly was created to check the results from the shell model and to look for internal stresses that are not viewable in the shell model. The results of this analysis were values below the 5850 psi tensile strength of the epoxy bond, with the highest values within a factor of safety of 4, showing that delamination of the fin brackets is not of concern (Appendix C.3 and E).

2. *Launch lugs*

The three launch lugs that secure the rocket to the launch rail are connected to the rocket body via specially designed launch lug arc clamps (Fig. A.3). These speciality arc clamps accept the launch lugs which incorporate two brackets each, for a total of six brackets, that are then held in place by two 18-8 stainless steel socket head screws per bracket. There are two potential points of failure: the 90° bends on the brackets, and the fasteners connecting the brackets to the launch lug clamps. Even if the geometric stress concentration was within acceptable levels for the brackets alone, running an extra launch lug assembly simulation in addition to the solo bracket analysis needed to be performed. Thus, the "Launch Lug" simulations took two forms, one analyzing just the bracket itself, and the other the entire lug/arc clamp assembly.

The first simulations performed were on the launch lug brackets and involved an intentionally inflated load scenario to confirm the location of the geometric stress concentration on the bracket. After this concentration area was confirmed, a filleted radius was added to the 90° angle of the bracket. An analysis was then performed in which the stress concentration area was verified to be mitigated by the fillet and produced a FOS to yield 31.1, much greater than the required factor of safety of 2. In the future, the Launch Lug brackets may be redesigned to save mass, with the fillet providing the structural support preventing it from becoming an area of concern.

The launch lug to coupling ring assembly analysis was the most complex and time consuming FEA performed. Over eighty surfaces had to be defined and 35 interactions between these surfaces had to be designed into the simulation. Singularity issues arose with the stainless steel fasteners that were modeled and ultimately the results show imminent failure of the assembly. This simulation showed that more expansive software might be needed for these analyses. Currently showing a max stress exceeding over 13.7 times the allowable stress value, future teams will need to either run further simulations or in-person structural testing (Appendix C.3 and F).

3. *Isotanks*

Using an equivalent thickness of 0.055" per the recommendations from McCloud and the NASA Isogrid Handbook, the isogrid tanks were modeled in Abaqus a few different ways. One

approach involved a complete cylinder model of equivalent thickness and two others were radial partitions of the same model. One separate simulation involved a partition of the actual isogrid tank for information regarding the location of the maximum stress on the ribbed portion of the tank's exterior. Results from the compressive and pressure loads in the equivalent thickness simulations had a maximum Von Mises stress value of 25.290 ksi and maximum deformation of 0.01520 inches (Appendix C.3 and G).

4. End caps

Modeling the end caps with the calculated equivalent thickness produced unrealistically high stresses (Fig. C.3.12) so the part was imported as a step file. The stress results of the imported model were still higher than the ultimate strength of aluminum (Fig. C.3.13). Although the FEA was not completely accurate, the high stress values prompted a closer look at the plate thickness and McCloud revisited the calculations [5]. The 0.25 in thick endcap had stresses of 93 ksi at the max internal pressure of the tank when the ultimate strength of 6061 is approximately 45 ksi. The end cap thickness was increased to 0.4 in which gave a factor of safety of approximately 3.17.

MDO

In February 2021 the length:diameter ratio in the MDO was changed by PSAS to 23.7:1 due to stability and other information determined by the sponsor. In May, the MDO was run with updated information from the LV4 Airframe and Propulsion teams. The airframe mass was 195.1 lbs compared to the MDO estimate of 242.6 lbs and the length was 24.5 feet compared to the now required 23.7. However, due to the interdisciplinary nature with the Propulsion Team, not all constraints were met, including an expected apogee of approximately 70 km (compared to the 100 km needed). The sponsor requested a change in constraints of LFETS velocities and an apogee of 52.5 km and the MDO was again updated. The results can be seen in Figure 5, with an expected apogee of 51.3 km. The sponsor is considering leaving the Base11 challenge and changing the requirements to a much lower apogee of 50 km, which can be achieved by the current design.

```
CONSTRAINTS
----------------------------
Largest angle of attack (c.f. < 8.0)         = 6.0492 deg
L/D ratio (c.f. < 25.0)                       = 24.5095
fin flutter ratio (c.f. > 1.0)                        = 34.9024
Sommerfield criterion (c.f. pe/pa >= 0.35)    = 1.1835
max acceleration (c.f. < 15.0)                = 3.7018 gs
TWR at lift off (c.f. > 2.0)                 = 1.2781
Lowest stability margin caliber (c.f. > 2.0) = 2.7481
speed when leaving launch rail (c.f. > 22.0)  = 21.6115 m/s
altitude at apogee (c.f. > 52.5)              = 51.3259 km
LFETS LOX velocity (c.f. < 9.144)    = 9.1456 m/s
LFETS IPA velocity (c.f. < 9.144)    = 7.6163 m/s
design thrust (ground level) (c.f. < 10000)    = 7254.0210 N
```

Figure 5: Current MDO outputs as of May 30, 2021 [1].

6. Final Status

Further refinement was done on the designs for each subsystem as part of the Version 3 phase of LV4. The current rocket airframe is approximately 24.5 feet long, which meets the current MDO constraint of 25 feet. The update of the MDO in concordance with the Airframe and Propulsion Teams shows that the apogee of 100 km can not be reached. The constraints are being reconsidered by the sponsor. A more feasible apogee of 50 km is being considered, which the MDO shows is reached by the current rocket design.

Arc clamp FEA simulations were run using parts drawn in Abaqus rather than true partitions of existing CAD solid model parts from Onshape. The next iteration recommendation is to partition the actual CAD modules and CAD arc clamps to reflect true geometry values and separation gaps that exist in the true models on Onshape. Although only slight changes should arise using these “truer” models, it would help with understanding exactly how the stress concentrations in these local regions behave based on clearance dimensions.

Reevaluation of the launch lug assembly needs to be performed in Abaqus or other FEA software. The singularity issues that arose from the bolted fasteners shows imminent failure but further verification of the model’s validity and set up in the program should be checked. It is likely some solution to modeling the launch lug assembly in a more simplistic way needs to be explored instead of modeling the interactions purely with solid models imported into the workspace. In addition, a separate FEA simulation should be performed by simplifying the loading experienced by the arc clamp portion of the launch lug to examine the contact interaction of arc clamp to the coupling rings. This could easily be done by modifying the current FEA simulation for the arc clamps by changing the load distribution.

Further modifications could then be made to the arc clamps and coupling rings to ensure structural integrity both while on the launch rail and during launch. Additionally, the launch lugs need modified fasteners that hold the brackets in place to make them more accessible by hand when the rocket is on the launch rail, as they will be located in a tight space and tightening or loosening may be difficult. Launch lugs also need to be re-evaluated for their areas of stress concentration if in the future slimming down the design of the brackets is deemed necessary.

Equivalent thickness models were used for the isotanks and their buckling failure test simulations in Abaqus. It is highly recommended that when some initial isotanks are manufactured and produced that next steps taken should be to physically test for failure these modules in a mode of buckling in addition to the physical pressure testing.

Additional future work includes modifying the ERS and RCS module to include complete recovery and reaction control systems. These will most likely include structural changes to accommodate the systems. The length of the IPA and LOX plumbing modules will also vary based on the needs of the propulsion team, and the flexibility in dimension of the composite module lends itself to this application. When the plumbing designs are finalized, the plumbing module can be fabricated to the appropriate length. Further work should be done to modify the thrust plate to better integrate with the engine and propulsion components.

CFD simulations were completed on four different fin shapes and on two nose cone shapes when the rocket is traveling at maximum dynamic pressure. The optimal fin shape for drag and pressure was found to be a diamond trapezoid. A 3.6:1 fineness ratio using the Von Karman ogive for the nose cone was chosen for optimization of weight and drag. Further work should also be done to determine the center of pressure of the different fin shapes by changing the angle of attack in the CFD simulation in order to further contribute to fin optimization and the MDO stability analysis.

References

[1] “LV4 MDO Simulation and Optimization,” Portland State Aerospace Society, retrieved February 2021. https://github.com/psas/lv4-mdo/tree/master/Simulation_and_Optimization

[2] “NASA CR-124075 REVISION A - ISOGRID DESIGN HANDBOOK.” *Https://Www.nasa.gov/Goddard*, MCDONNELL DOUGLAS ASTRONAUFILS COMPANY, Feb. 1973, femci.gsfc.nasa.gov/isogrid/NASA-CR-124075_Isogrid_Design.pdf.

[3] Deng, F., Liu, J., Shen, C., Huang, W., 2014, ”Novel Approach for Design of a Waverider Vehicle Generated from Axisymmetric Supersonic Flows Past a Pointed Von Karman Ogive”, Aerospace Science and Technology, Vol 42.

[4] Iyer, A., Pant, A., Aug 2020, “A Review on Nose Cone Designs for Different Flight Regimes”, International Research Journal of Engineering and Technology, Vol. 7, Issue 8.

[5] “LV4 Isotank,” Portland State Aerospace Society, retrieved January 2021. https://github.com/psas/lv4-isotank

[6] “Spalart-Allmaras Turbulence,” STAR-CCM+ User Guide, Siemens, retrieved February 2021.

Appendices

Appendix A: Supplemental Images

Figures A.1 through A.12 show current (V3) images of the rocket components for LV4.

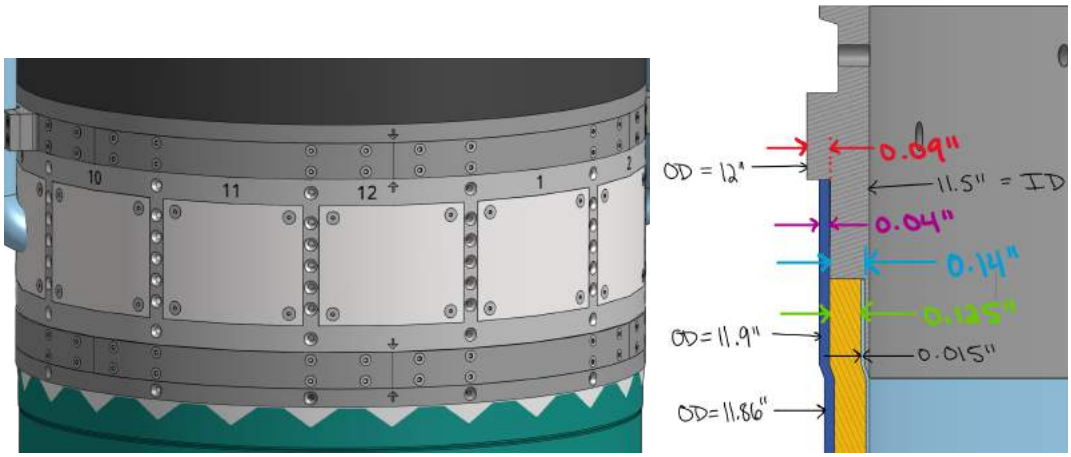

Figure A.1 LEFT: Close-up of passthrough module joining fin can and LOX tank with racepipe clamps shown centered above windows 9 and 3 and the arrow marking the seam between two arc clamps. RIGHT: Section view of V2 coupling ring with composite fiber "sandwich" attached.

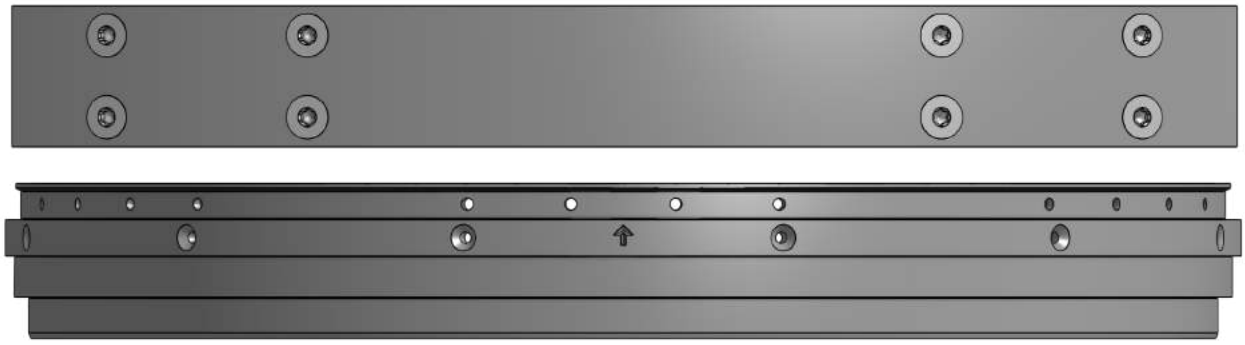

Figure A.2 TOP: Current Arc Clamp assembly. BOTTOM: Current coupling ring with positional arrow shown.

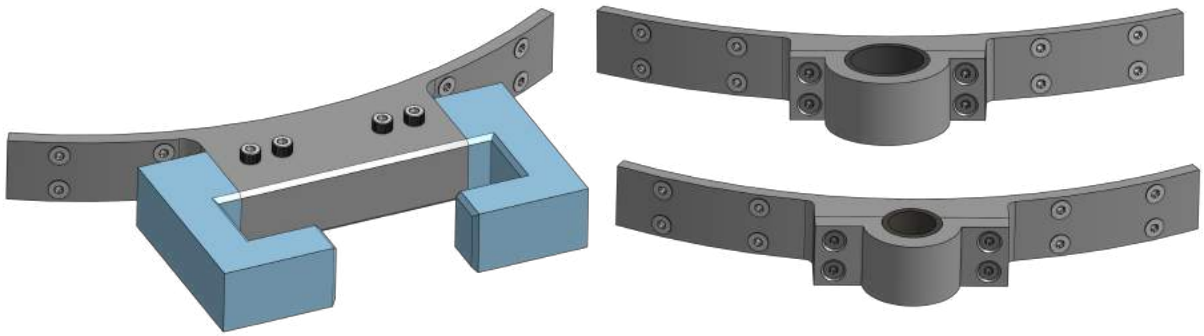

Figure A.3 LEFT: Current Launch Lug assembly. RIGHT TOP: ¾ inch racepipe clamp. RIGHT BOTTOM: ½ inch racepipe clamp.

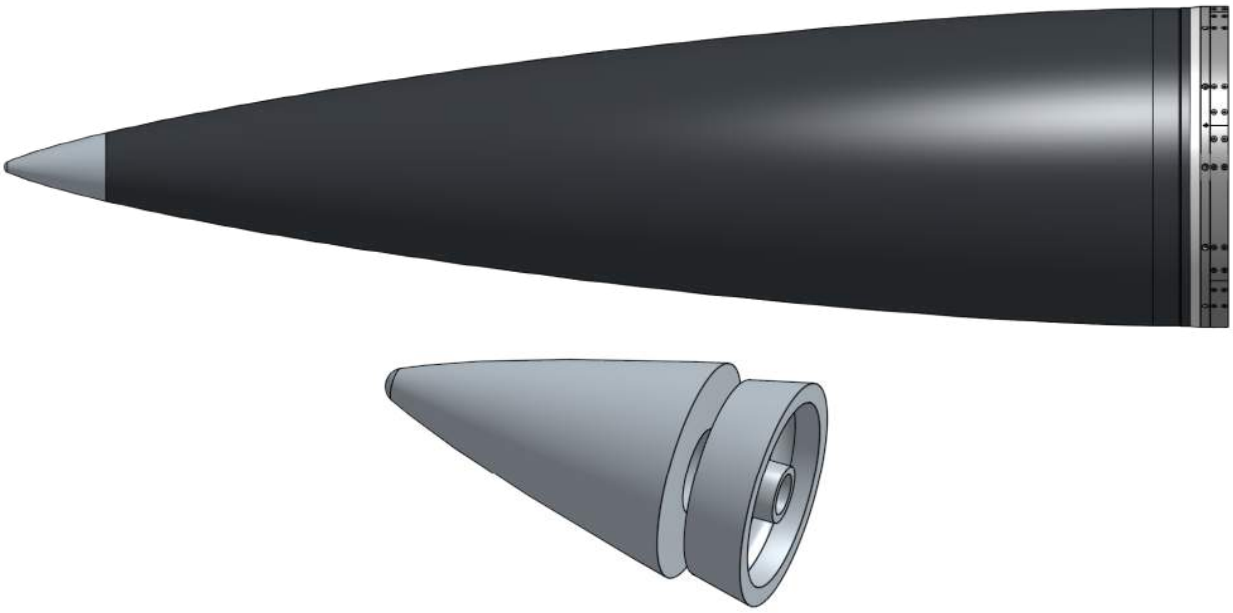

Figure A.4 TOP: Nose cone with Von Karman ogive and flat cylindrical section showing nose cone tip. BOTTOM: Nose cone tip with wedge for layups.

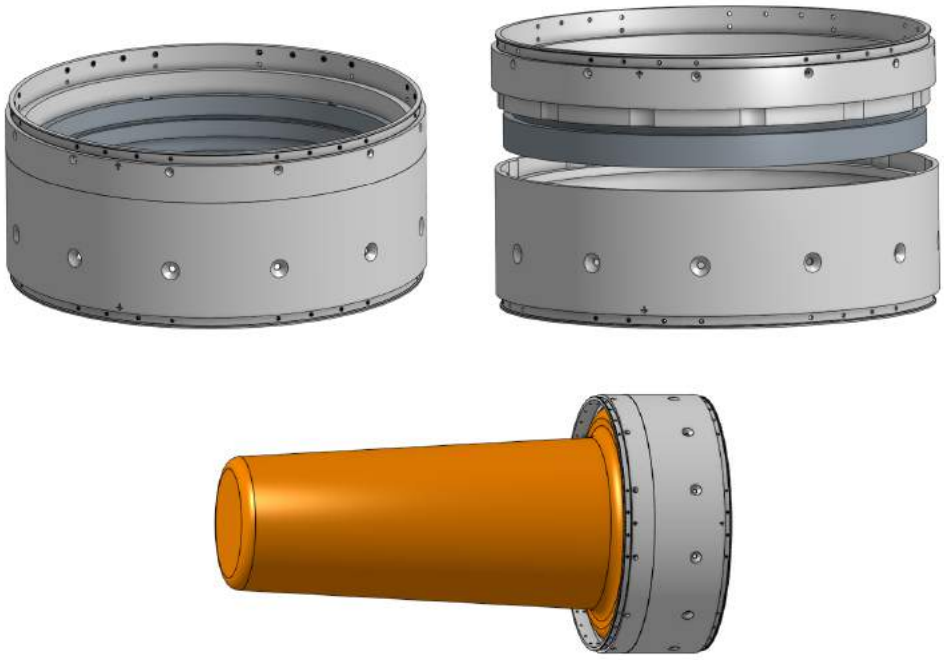

Figure A.5 TOP LEFT: LV3.1 ERS module subassembly. TOP RIGHT: LV4 ERS two-piece module with slide connectors and twist coupling shown. BOTTOM: ERS showing the dummy recovery system used to replicate mass for the MDO program

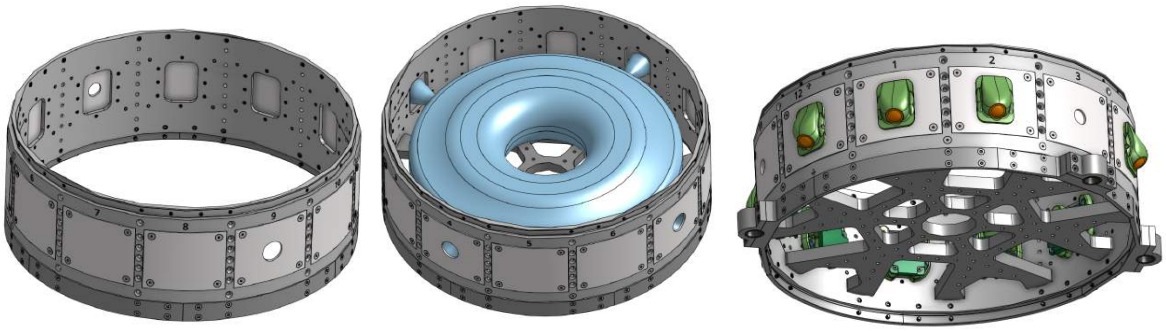

Figure A.6 LEFT: Current Passthrough module. MIDDLE: Current RCS Module. RIGHT: Current Camera Module

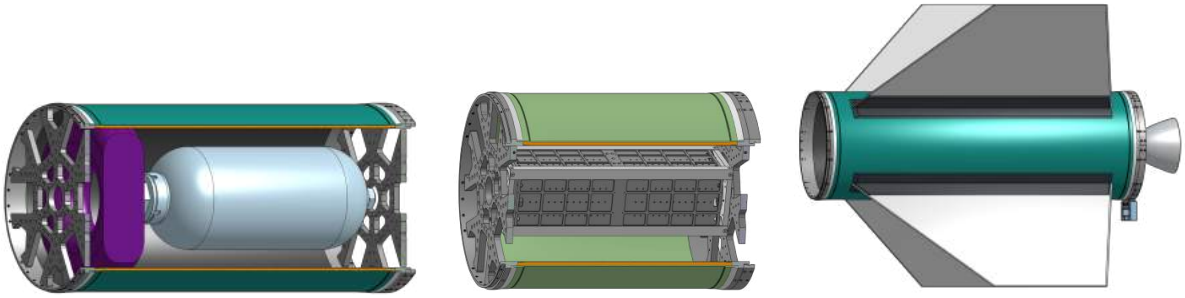

Figure A.7 LEFT: Current N2 module with nitrogen tank and plumbing mass. MIDDLE:Current avionics module with CubeSat and cradle. RIGHT: Current fin can module with engine and thrust plate.

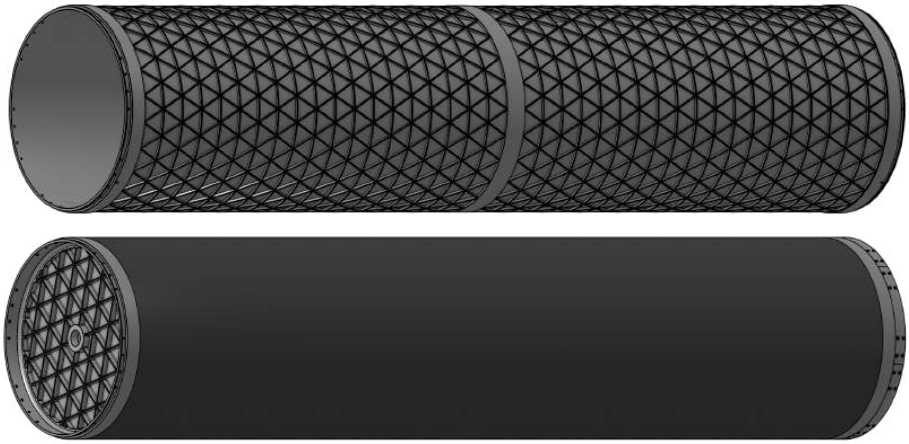

Figure A.8: One of two aluminum isogrid fuel tank modules that will house liquid oxygen and isopropyl alcohol. This is a new design for LV4 that was not incorporated in LV3.1. TOP: V3 isotank with correct cell and rib size and a center welding margin. BOTTOM: The tank wrapped in a carbon fiber aeroshell with the end caps welded onto the ends.

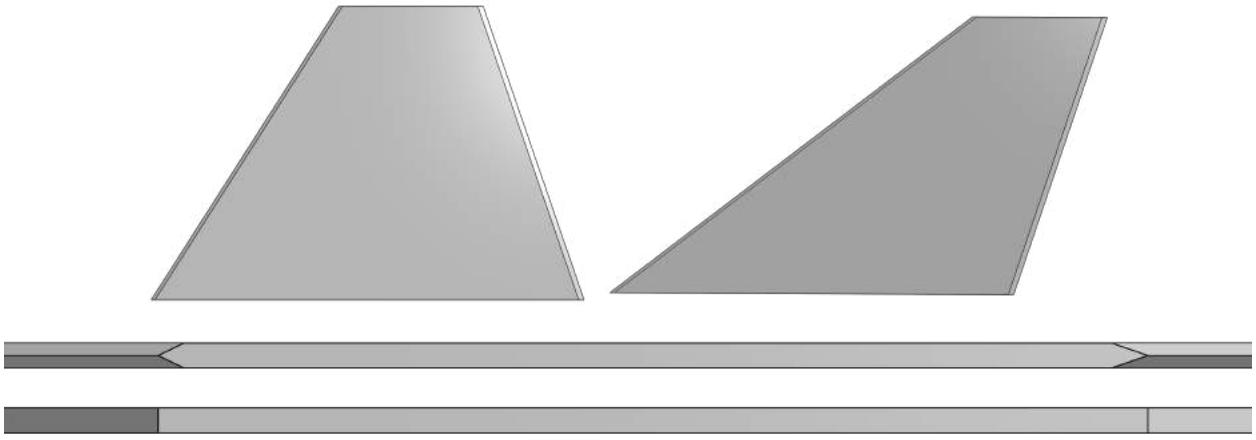

Figure A.9 TOP: Trapezoidal fin shape vs swept fin shape. BOTTOM: Diamond cross section vs rectangular cross section.

Figure A.10: Example of one race pipe that is delivering compressed nitrogen to the LOX tank. These racepipes will have ID dimensions of ½", ½", and ¾" for the Isopropyl alcohol pipe, Nitrogen gas pipe and the liquid oxygen pipe, respectively.

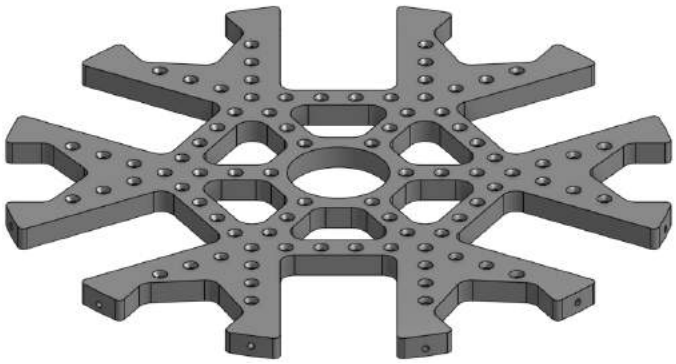

Figure A.11: Bulkhead for the final version.

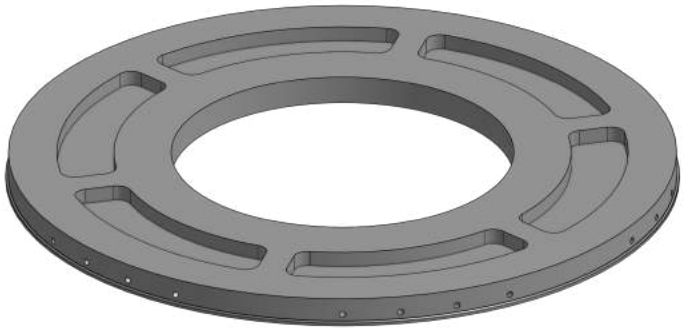

Figure A.12: Current thrust plate design acting as a placeholder until future work with the Propulsion Team.

Appendix B: Catalog of Design Artifacts

B.1: OnShape CAD Models
https://cad.onshape.com/documents/ed9790ce496523101fa7a99d/w/592c291964cc7221c224492b/e/f9d1d52b285b49087c7c9a88

B.2: Google Drive
https://drive.google.com/drive/folders/1boyj5U7ekgyVVB02GtFPS5idkuqNaI-J?usp=sharing

- UTEAP (Undergraduate Team Experience Award Program)
    - Airframe Material List
- Analytical Models and Results
    - CFD
    - FEA
- Project Management
    - Airframe Risk Analysis Workbook
    - Gantt Chart
- Team Communications
    - LV4 MDO Meeting Notes (Sponsor Meetings)
    - LV4 Capstone Notes (Team Meetings)
- Presentations and Reports

Appendix C: Concept Analysis

C.1: Design Progress

This section details the design progress of the subsystems of LV4 over the length of the capstone.

1: Nose Cone

V1 had an 8 inch flat cylindrical section matching LV3.1. This space was used in LV3.1 to accommodate the components for the recovery system. Due to LV4's increased diameter and the corresponding increased volume within the nose cone, this section was reduced to 1 in. which leaves enough space for the recovery system and also will help to reduce mass. The nose cone also went from a carbon fiber tip in V1 to a blunted aluminum tip with an aluminum composite wedge to clamp against the nose cone for composite layup manufacturing (Fig. C.1.1).

Figure C.1.1 Top: V1 of the nose cone showing a carbon fiber tip, 8 inch flat cylindrical section, and no coupling ring attached. Bottom: Final version of the nose cone with a 1 inch flat cylindrical section, aluminum tip, and coupling ring attached.

2: ERS

V1 did not include any simulated components or the twist coupling ring, but these were produced for the final version. For the final version the bulkhead hole placement was changed, alignment arrows were added, and a dummy recovery system was added to replicate the mass and volume for the MDO.

3: Passthroughs

Initially the V1 Camera Module and the V1 Passthrough Module had their own respective designs. The Passthrough Module took 3 iterations to arrive at its current state based on a modified Camera Module. The once separate designs now sharing the same modular design will lower the cost of manufacturing by having a single design that will perform the multiple functions of these different sections. In turn, this would also help allow for more access to the

internal components of the rocket body through the window ports before covering them up with their respective covers compared to before where the only access was from either end of the modules. Figures C.1.2 through C.1.4 show the progress of the RCS, camera, and general passthrough modules.

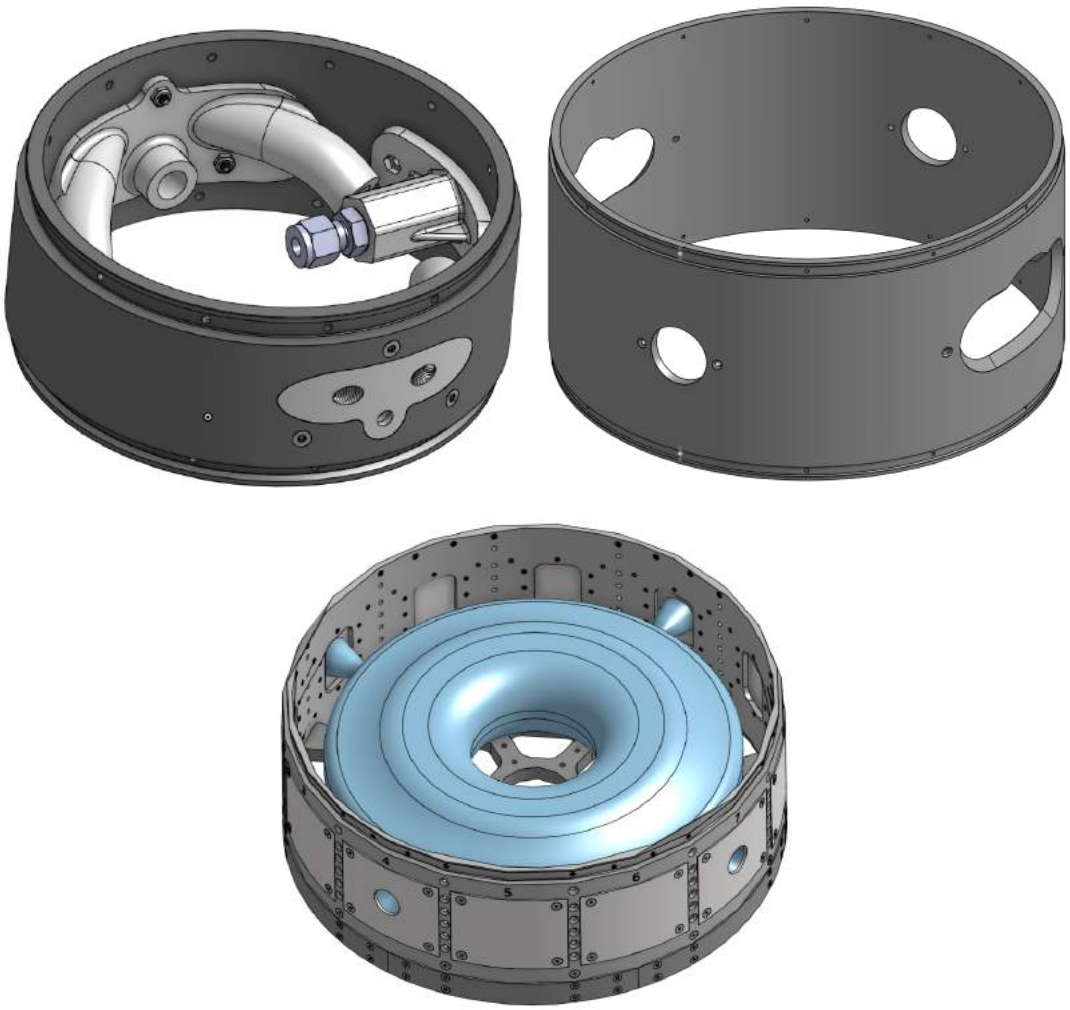

Figure C.1.2: The Roll Control System module composed of windows that will allow the internal pressurized nitrogen gas nozzles to correct the orientation of the rocket mid-flight. TOP LEFT: the previous RCS module from LV3.1. TOP RIGHT: V1 of the LV4 RCS module. BOTTOM: V3 RCS with its simulated internal N2 gas nozzles/plumbing.

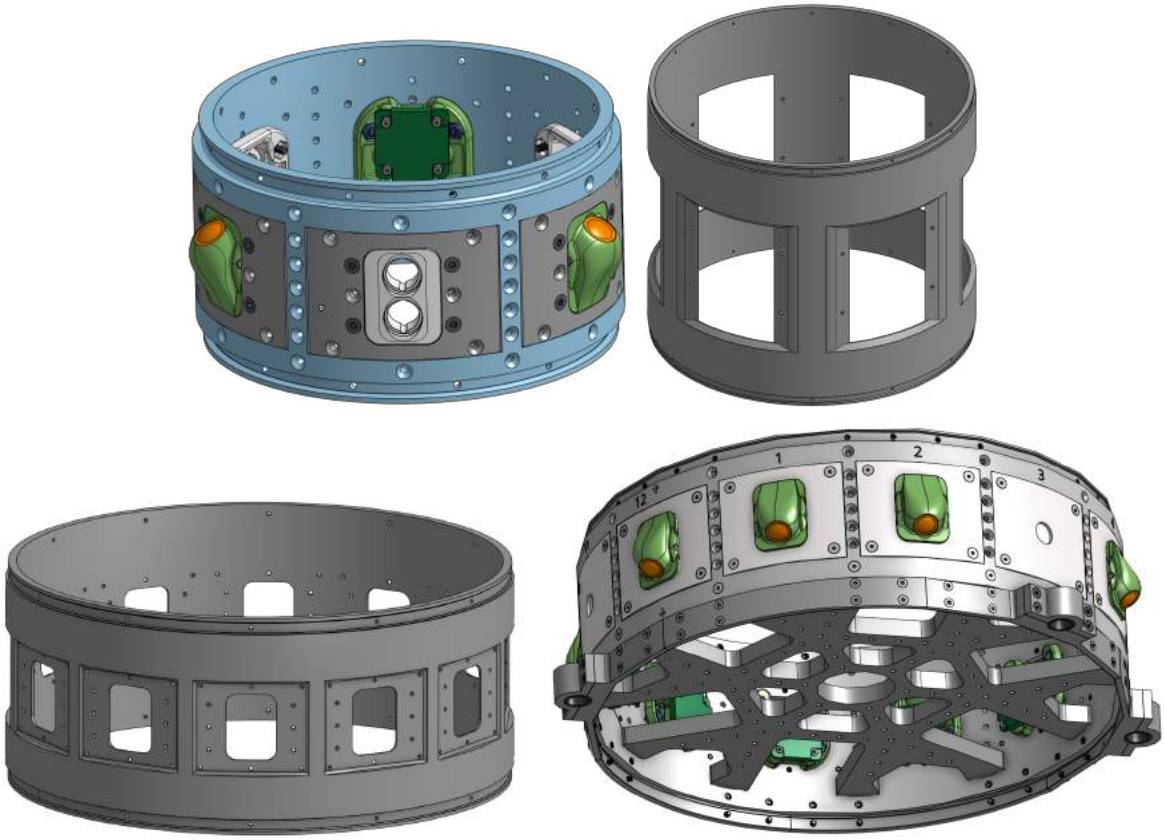

Figure C.1.3 TOP LEFT: LV3.1 Camera module TOP RIGHT: V1 design of the camera module for LV4. BOTTOM LEFT: V2 houses 12 windows, 9 of which will be used for video camera placement while the other 3 will be covered with 3D printed window covers. BOTTOM RIGHT: V3 of the LV4 Camera Module in its subassembly form complete with bulkhead, window coverings and onboard video cameras. The V3 camera module also houses 12 columns of countersunk through holes to allow for easy placement of the bulkheads inside the module.

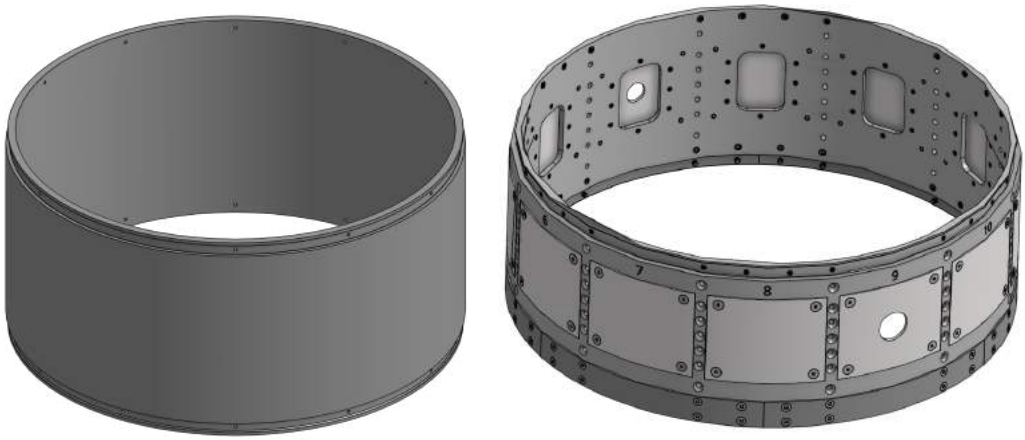

Figure C.1.4 LEFT: V1 of the Passthrough modules. RIGHT: V2 is a copy part of the camera module with its needed window coverings installed.

4: Modules

V1 was a scaled-up version of LV3.1. V2 incorporated a thinner Nomex layer, with the composites matching the contours of the coupling rings, and added a 3-D printed chamfer at the composite/coupling ring interface (Fig. C.1.5). For V3, lengths of the composite were adjusted and the updated V3 coupling ring used. A mass representation of the RCS plumbing and a COTS nitrogen tank are included in RCS, a CubeSat and cradle are included in Avionics (Fig. C.1.6), and an engine is included in the fin can.

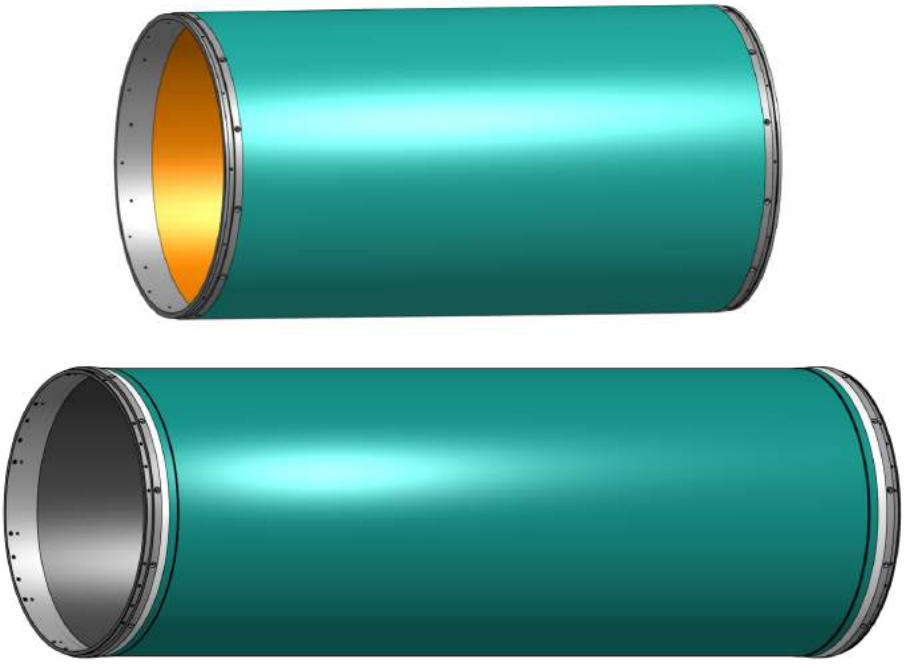

Figure C.1.5: Carbon Fiber Module. The module is a layered "sandwich" design of carbon fiber and Nomex, bonded to coupling rings. This design is a scaled up version that will be tested with LV3.1. TOP: V1 lacked the inner carbon fiber layer and contours of the coupling ring. BOTTOM: V2/3 was updated in length with realistic contours where the layers connect to the coupling rings and a 3-D printed chamfer at the composite/coupling ring interface.

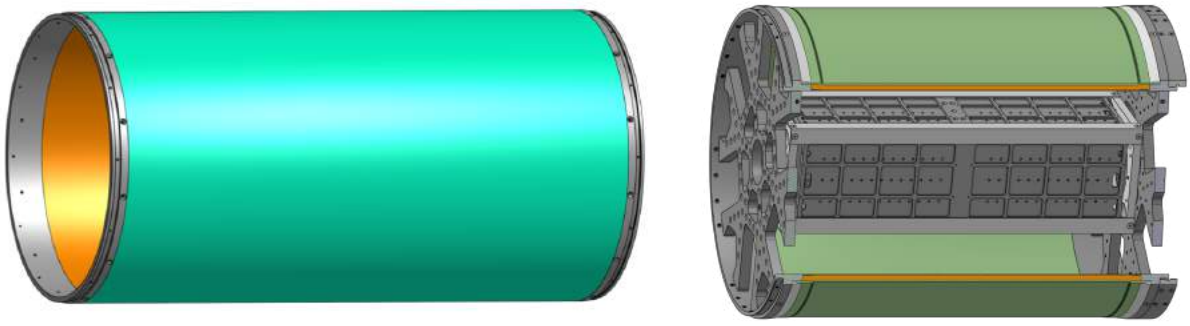

Figure C.1.6: Similar in design to the carbon fiber module, the avionics module is made with fiberglass instead of carbon fiber, which interferes with ground communication. LEFT:V1 lacked the inner fiberglass layer and contours of the coupling ring. RIGHT: Section view of V3 fiberglass avionics module, showing mass representation of cubesat frames and cradle.

5: Isotanks

The original design was modeled on a half-inch thick cylinder with a wrap feature. The design for V1 had to be made for a quarter-inch thick tank and follow the parameters in the MDO. The isogrid had to be modeled as a helical sweep feature in order to achieve parallel rib surfaces for machining. V2 refined the model and added some features that were missing from V1, such as a center weld margin and a carbon fiber aeroshell (Fig. C.1.7). The isogrids were challenging to model in Onshape due to the computationally intense geometry. V3 was planned to be modeled as a wrap to make the modeling and parameters simpler but Onshape did not handle the geometry well so V3 did not change from V2. The end caps were added in V2 with a thickness of 0.25 in. After modeling in FEA, the end caps were re-evaluated and changed to a thickness of 0.4 in.

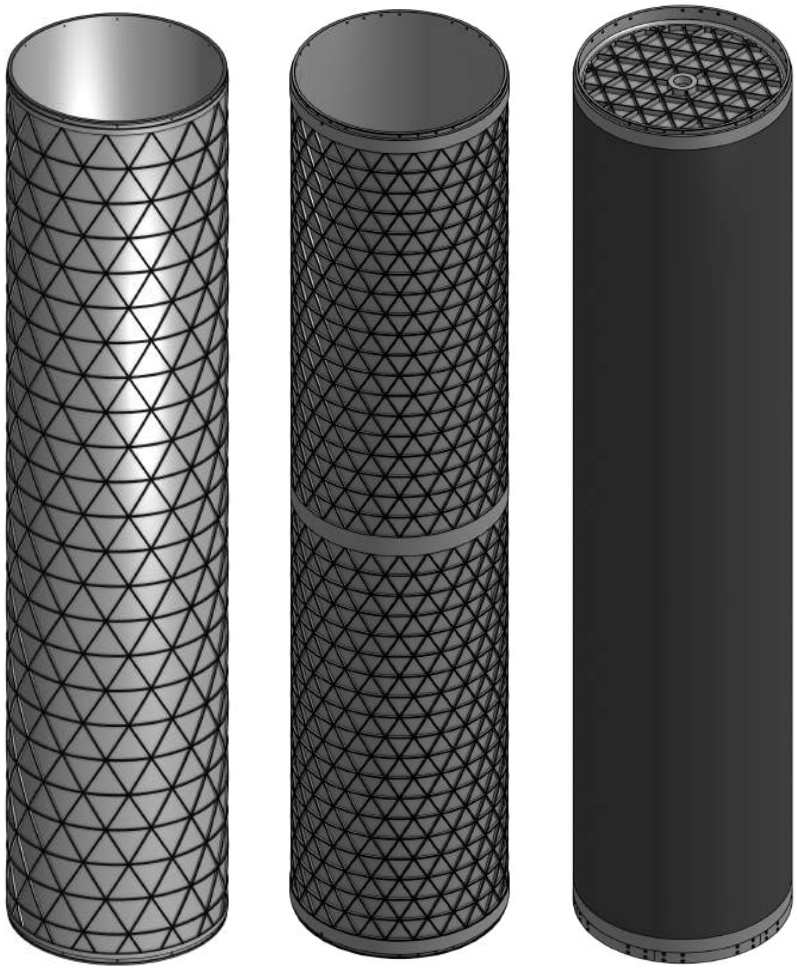

Figure C.1.7: One of two aluminum isogrid fuel tank modules that will house liquid oxygen and isopropyl alcohol. This is a new design for LV4 that was not incorporated in LV3.1. LEFT: V1 isotank with arbitrary cell and rib size. MIDDLE: V3 isotank with correct cell and rib size and a center welding margin. RIGHT: The tank wrapped in a carbon fiber aeroshell with the end caps welded onto the ends.

6: Fins

V1 fins were scaled up from the LV3.1 design. For V2, different geometries and cross sections were used for CFD analysis. With results of the CFD favoring the trapezoidal diamond cross section, V3 used this geometry with reduced dimensions with surface area matching the MDO requirements (Fig. C.1.8).

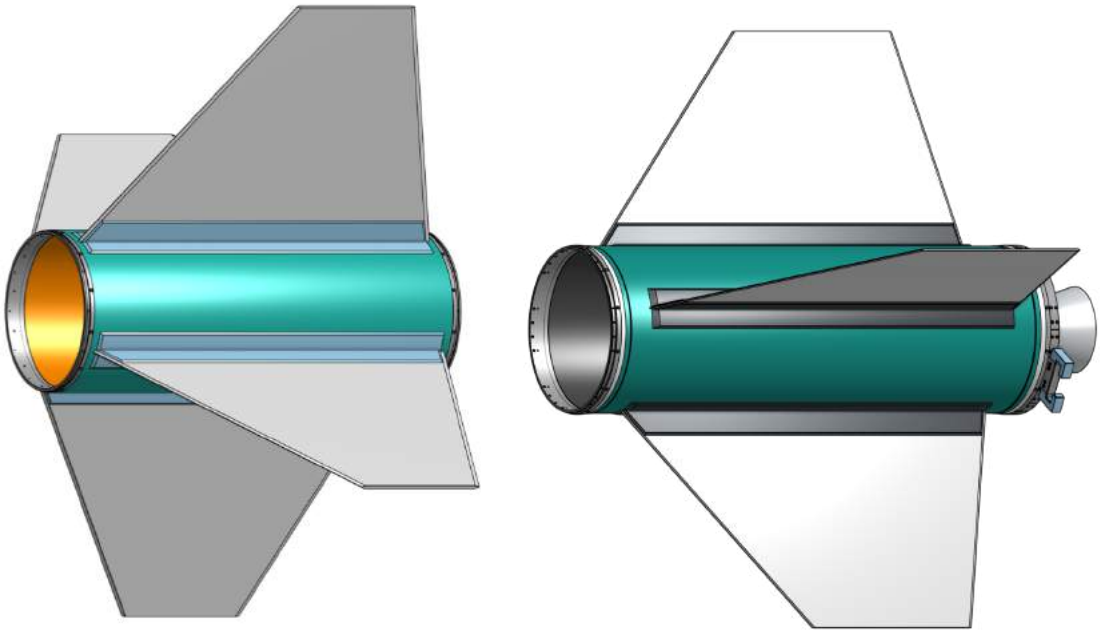

Figure C.1.8: Carbon fiber fin can module. Note the carbon fiber brackets used to bond the fins to the composite module. LEFT: V1 design uses scaled up LV3.1 trapezoidal diamond cross-section fins. RIGHT: V3 uses updated V3 composite module with CFD optimised fin geometry. Note mass representation of the engine.

Coupling Rings and Arc Clamps

For V1, the coupling rings and arc clamps were scaled up to accommodate the 12 in OD and 11.5 in ID. This change showed that they had to be updated because the walls in which the arc clamps attach to were too thin to be feasible. V2 of the coupling rings and arc clamps have small improvements in CAD and dimensions with more and larger fastener holes and accommodate the smaller Nomex size which results in the "sandwich" no longer being flush with the OD. While changing the ID would fix this problem, it would affect the thickness of the arc clamps and their coupling ring interface. Our sponsor requested that to solve this issue we should create 3D printed chamfers to glue into the gap between the OD of the "sandwich" and the OD of the ring.

V3 has hole sizes in CAD that correspond to the untapped diameter of the holes, as they will need to be tapped for #4-40 helicoils. The CAD assembly includes these helicoils and all necessary fasteners. A note will need to be placed on the manufacturing drawings to tap the holes for the helicoils. The final coupling rings also include engraved arrows that mark the location of the seam between the first and last arc clamps to aid with assembly and alignment. Unused holes (as determined by placement of the arc clamps in relation to passthrough windows) were removed from the rings (Fig. C.1.9). There are small clearance distances of 0.005 and 0.01 inches between the surfaces of the arc clamps and the surfaces of the coupling ring, except for

the faying surface (the chamfered “wedge” edges). This clearance allows for manufacturing defects as well as small translational misalignments between two modules. To minimize this misalignment during assembly, one can also first loosely attach 3 equally-spaced clamps, then check that the exposed portions of the rings are flush while tightening the clamps, then attach and tighten the remaining clamps. The chamfers were changed to 20 degrees due to manufacturing limitations. V1 compared to V3 is shown in Fig. C.1.10.

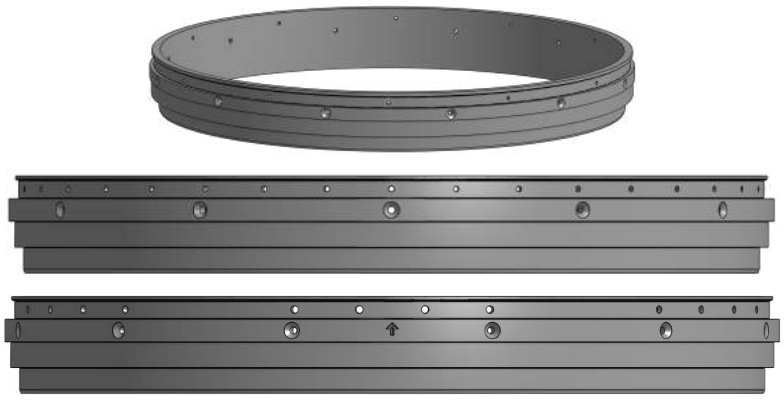

Figure C.1.9 TOP: V1 coupling ring with arc clamp holes on top and bulkhead holes in the middle to allow for attachment of bulkheads. MIDDLE: V2 coupling ring with additional fastener holes added. BOTTOM: V3 coupling ring with unused fastener holes removed and arrow added for assembly alignment and placement of arc clamps.

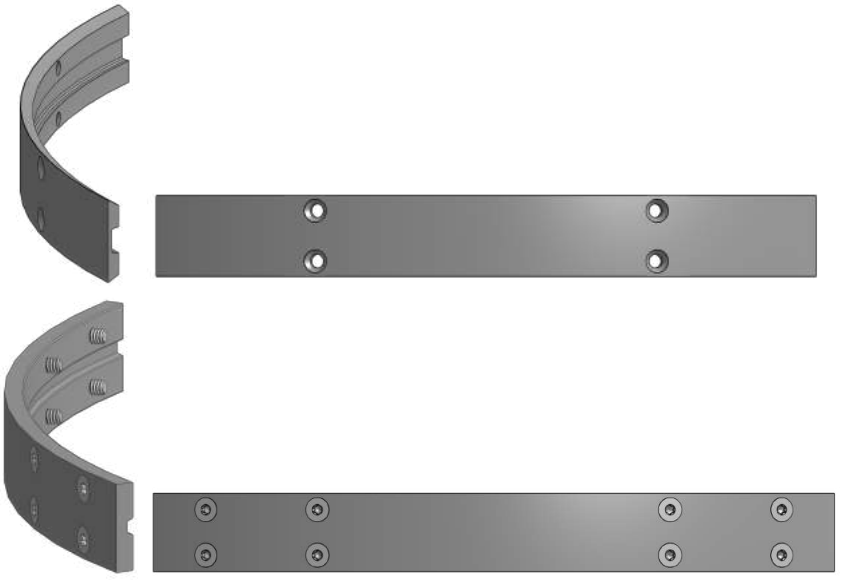

Figure C.1.10 TOP: V1 standard arc clamps with holes to attach to the coupling rings. BOTTOM: V3 arc clamps with additional fastener holes, modified slot dimensions, and fasteners added.

a. Launch Lugs

The V1 design modified the initial brackets (done by a previous team) to be inserted into the lug allowing for the bending force to be transmitted to the lug/arc clamp rather than to the fasteners. V2 increased the number of fasteners in each arc clamp from 4 to 8 in order to accommodate for the thinner walls of the arc clamps compared to LV 3.1 and minimize chance of fastener shearing in the launch lug assemblies when holding the rocket horizontally on the launch rail. V3 includes additional fillets on the brackets to provide needed structural strength as determined by FEA results (Fig. C.1.11).

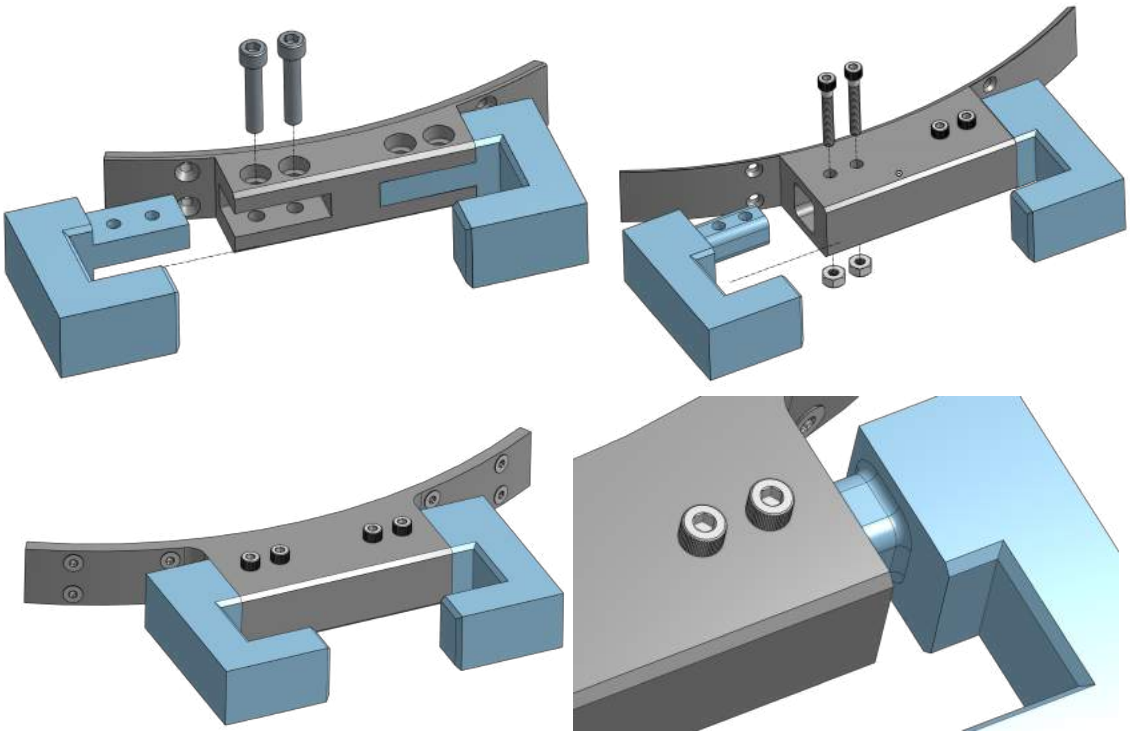

Figure C.1.11 TOP LEFT: Previous launch lug assembly built into an arc clamp with removable brackets shown in blue held in place with socket head fasteners. TOP RIGHT: V1 Launch Lugs assembly with removable brackets now inserted into a slot. BOTTOM LEFT: V3 Launch Lugs assembly with four more fasteners added. BOTTOM RIGHT: Close-up view of fillet added for V3 launch lug

b. Racepipe Clamps

Hose clamps and zip ties were considered for racepipe clamps but were ultimately decided against by our sponsor, who felt that machined clamps would provide better vibrational damping.

Miscellaneous

a. Bulkheads

The bulkheads were initially modeled similarly to the bulkheads used in LV3.1. V1 took advantage of the symmetry of the part and made the model with some variation from the LV3.1 version. V2 and made incremental changes to the size of the features with the goals of reducing weight. V3 also made a thickness change from 0.5 inch to 0.4 inch to accommodate some features in the rocket modules and with the added benefit of further weight reduction (Fig. C.1.12).

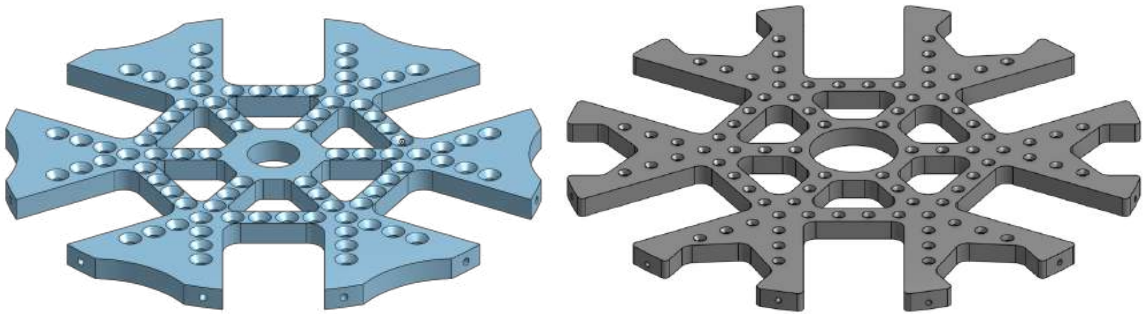

Figure C.1.12 LEFT: V1 Bulkhead. RIGHT: Bulkhead for the final version.

b. Thrust Plate

An initial thrust plate was created for V3 based on the LV3.1 thrust plate. It acts as the bottom-most coupling ring to allow for placement of the bottom-most launch lug. Modifications were made to extrude the outer wall to provide more volume for the fasteners to thread into (Fig. C.1.13).

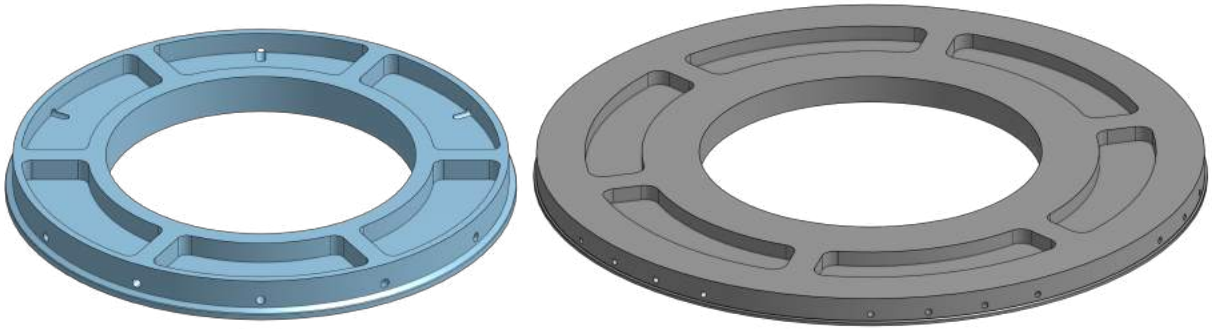

Figure C.1.13 LEFT: LV3.1 thrust plate. RIGHT: LV4 thrust plate with extruded outer walls and fastener hole pattern matching that of a coupling ring.

C.2: Images of CFD Analysis

Figure C.2.1 shows Computational Fluid Dynamics streamlines for the four fins when traveling at maximum velocity. Table C.2.1 shows the results of drag force and maximum frontal pressure for four fin shapes traveling at maximum dynamic pressure. Figures C.2.1 through C.2.4 show the velocity scene, drag force plot, and streamlines for a simplified analysis of the nose cone without an attached rocket body. Tables C.2.2 through C.2.4 show the results and solvers used in the nose cone analysis. This analysis was done at the simulation speed of 699.5 m/s (Mach 2.348) and an altitude of 9.9 km (Max Q conditions).

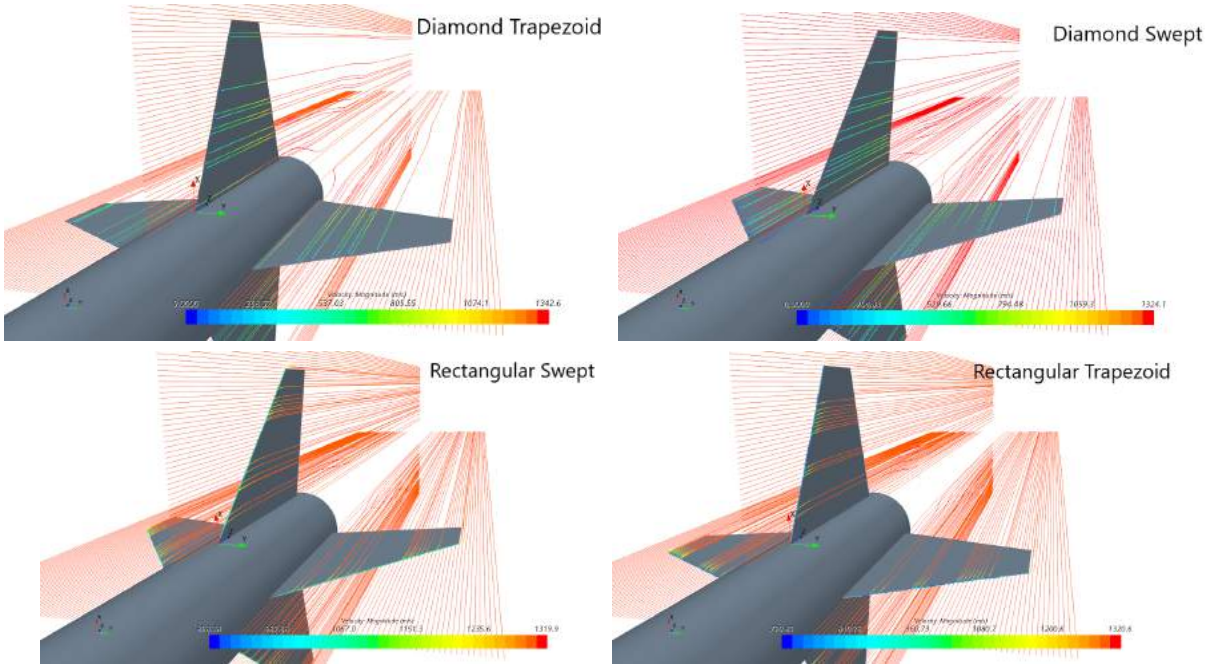

Figure C.2.1: Streamlines around the four fin shapes when traveling at maximum velocity.

Table C.2.1: Summary of Drag Force and max frontal pressure for the four fin shapes at max dynamic pressure.

	F_D (N)	P (psi)
RT	274.67	31
DT	45.89	5.8
RS	132.74	13.8
DS	93.05	6.05

Table C.2.2: Boundary conditions and initial values used for the nose cone simulations in Star CCM+.

Property	Value
Static Temperature	220.8 K
Density	0.356 kg/m^3
Dynamic Viscosity	1.4124 x 10^{-5} Pa-s
Absolute Pressure	22547 Pa
Thermal Conductivity	0.02016 W/m-K
Mach number	2.348
Velocity	699.5 m/s

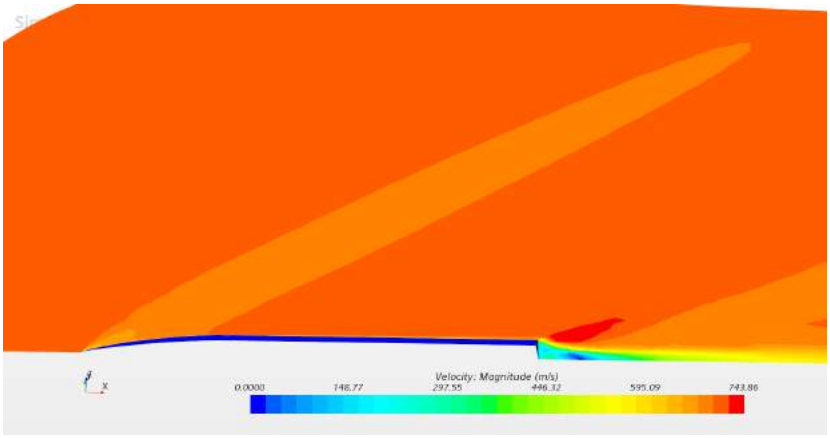

Figure C.2.2: Velocity scene in Star CCM+ showing bow shock of the nose cone traveling at 699.5 m/s (Mach 2.348).

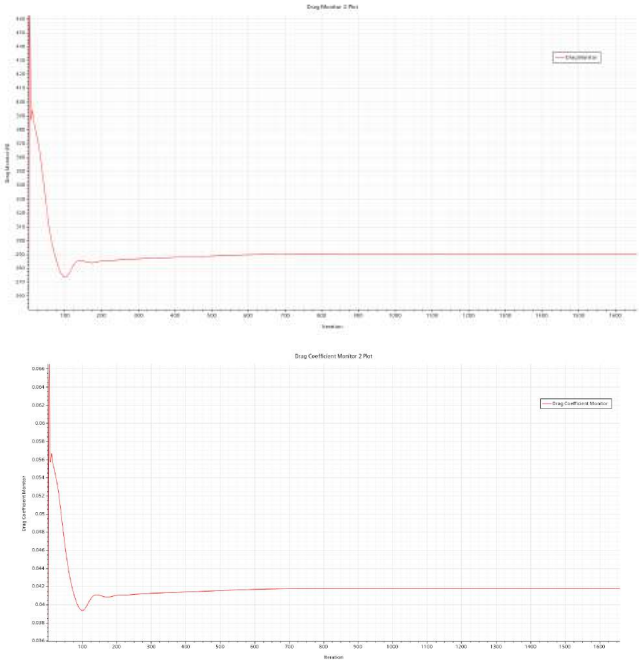

Figure C.2.3 Top: Drag Plot of the nose cone at MAX Q showing a drag force converging at 290.6 N. Bottom: Drag coefficient plot converging at 0.042.

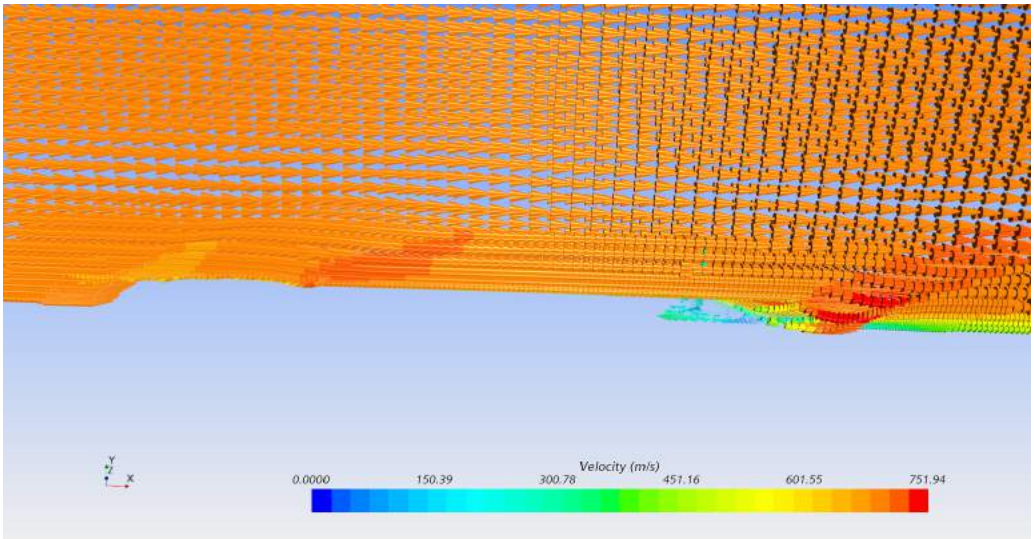

Figure C.2.4: Streamlines around nose cone.

Table C.2.3: Key CFD results from comparing base case with 5:1 fineness ratios.

	Base Case (3.6:1)	**5:1**
Length	43.5 in	60 in
Drag	290.6	246.2
Drag Coefficient	0.0418	0.0293
# of Iterations	1657	1557
Mass	11.30 lb	28.74 lb

Table C.2.4: Solvers used in Star CCM+ for the nose cone simulations.

Selected Solvers	**Auto-Selected Solvers**
Three Dimensional	All Y+ Wall Treatment
Coupled Flow	Solution Interpolation
Steady	Wall Distance
Ideal Gas (air)	Gradients
Spalart-Allmaras Turbulence (standard)	Reynolds-Averaged Navier Stokes (RANS)

C.3: Images of FEA

Figures C.3.1- C.3.14 show the range of simulations FEA was performed on.

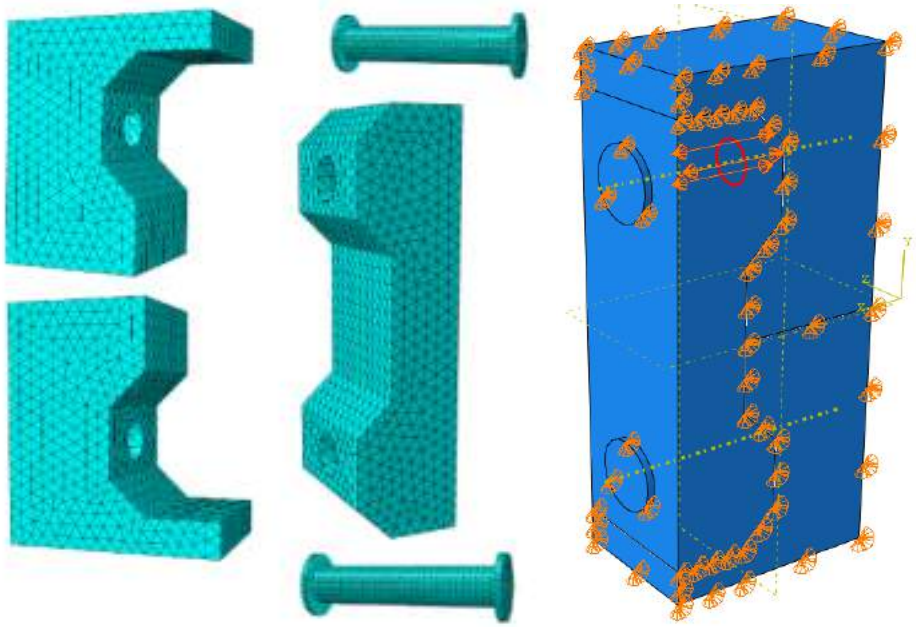

Figure C.3.1 LEFT: The individual parts designed to be used in the arc clamp FEA simulation and RIGHT: The assembly image in Abaqus with its interaction properties and surface definitions outlined prior to simulation submission

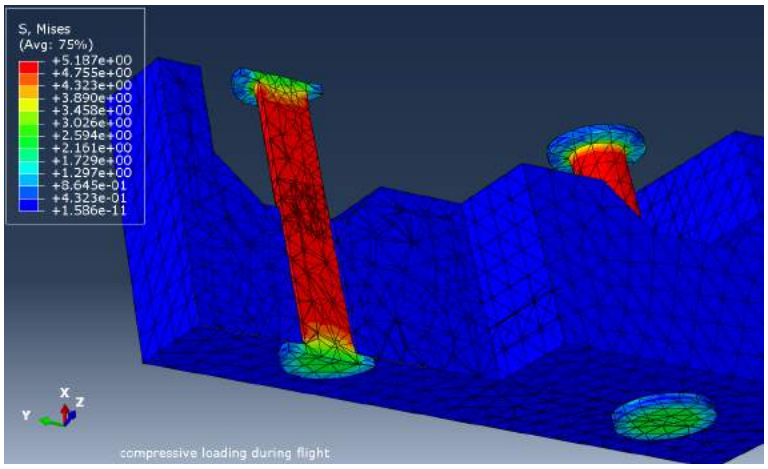

Figure C.3.2: Cutaway view of a compressive in-flight load simulation result of the arc clamps max. Von Mises stress. This loading scenario represents the compressive loading that the modules, arc clamps, and fasteners experience during flight. Values for the max. Drag and max. Thrust loads were pulled from the MDO at their respective time during flight for use in this simulation.

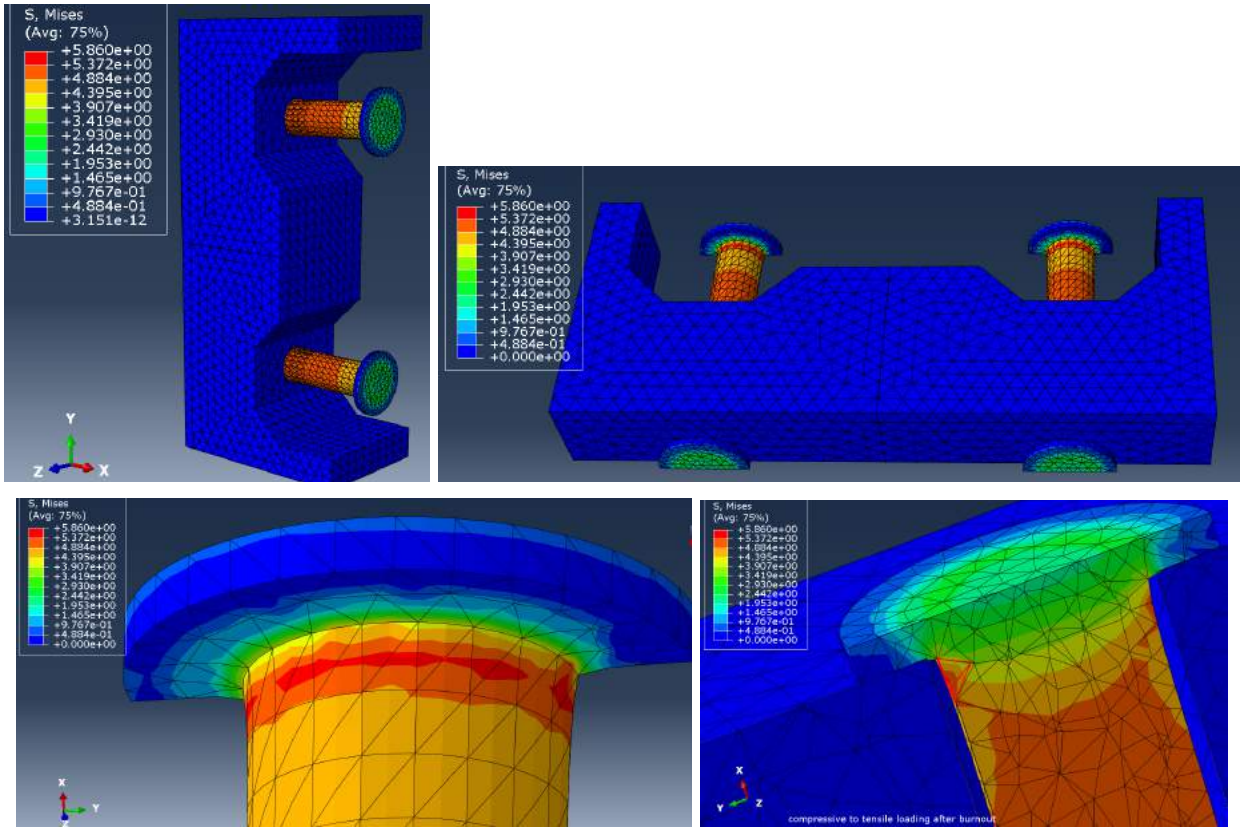

Figure C.3.3 TOP LEFT: Full assembly of the Arc clamp revealing the bolts and modules it is attached to. TOP RIGHT: Cutaway view of a dynamic load simulation result of the arc clamps max. Von Mises stress. BOTTOM LEFT: This loading scenario represents the dynamic shifting of compressive to tensile loading that the modules, arc clamps, and fasteners experience at the instant of burnoff. Values for the max. Drag and max. BOTTOM RIGHT: internal fastener stresses being depicted for the same assembly analysis. Thrust loads were pulled from the MDO at their respective time during flight for use in this simulation.

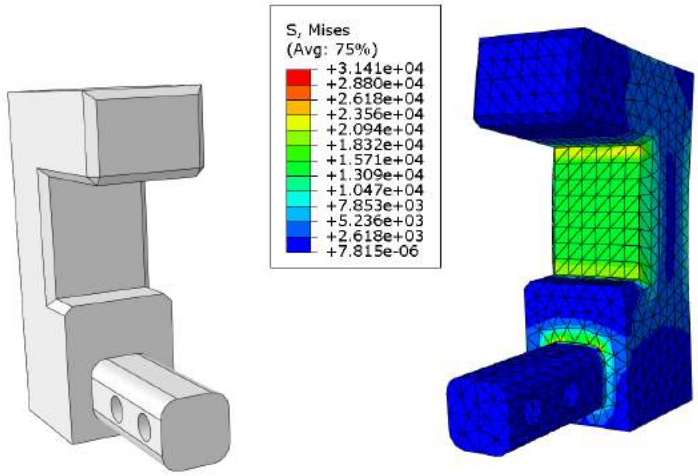

Figure C.3.4 LEFT: The first iteration of the Launch Lug Bracket solid model that was brought into Abaqus for simulation. RIGHT: the first simulation results from the model were performed without the fillet and a hypothetical inflated load was applied. This was done to verify the areas of its stress concentration which were confirmed as the areas around the 90-degree angles formed.

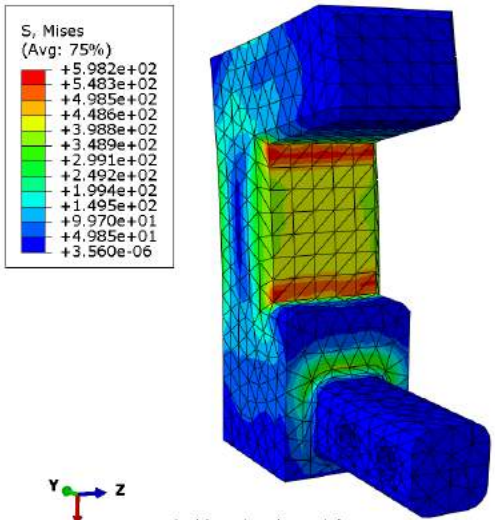

Figure C.3.5: Second simulation of the Launch Lug Bracket which produced a max. Von Mises stress value of 1.124 ksi resulting in a factor of safety to yield of 31.1. This loading scenario represents what the launch lug bracket would actually experience when the rocket is hanging from the launch rail by the six total launch lug brackets in its dry weight form of 202.5 lbm, meaning no fuel has been added yet.

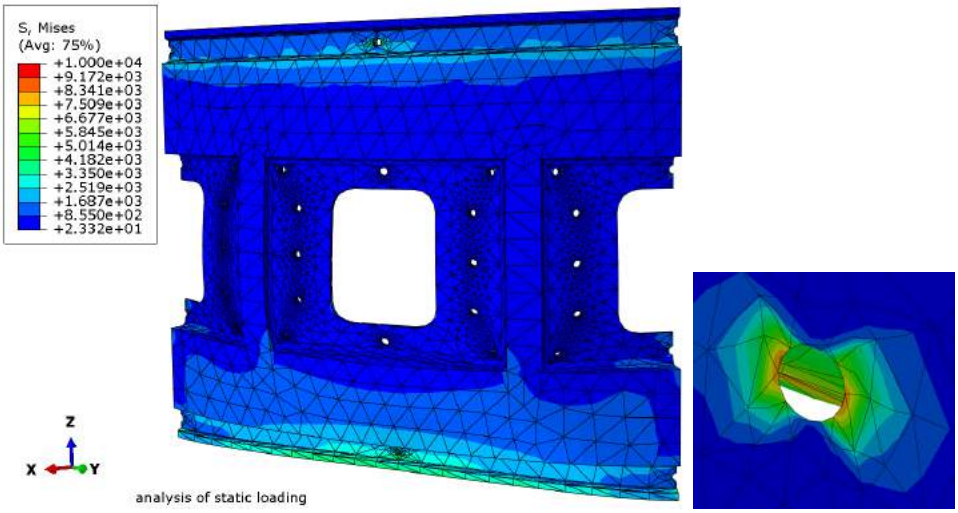

Figure C.3.6 LEFT: Abaqus FEA simulation results of the V2 camera module partition that was used for load analysis on the compressive loading acting on the module body. RIGHT: the bolt holes that support the fasteners. Max. Von Mises stress in this specific partition was 10.00 ksi.

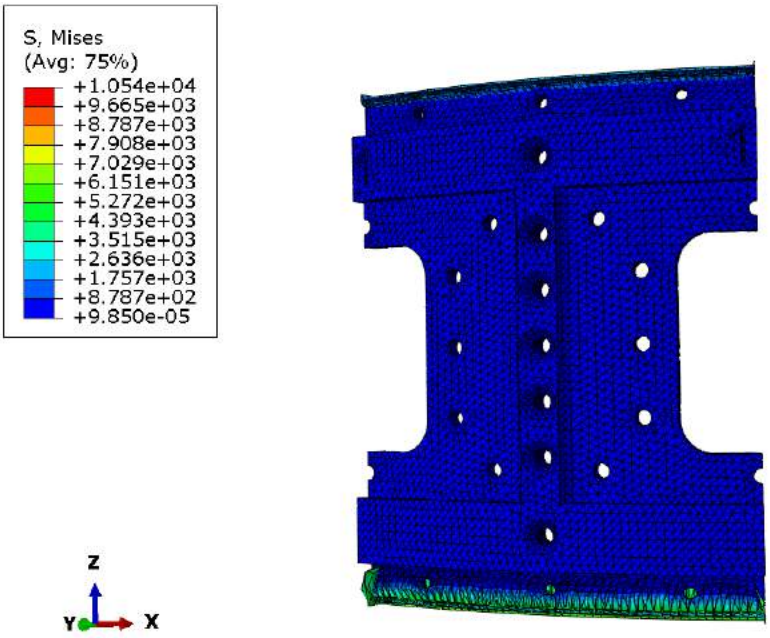

Figure C.3.7: A variation partition of the V3 camera module that reports slightly higher max. Von Mises Stress value of 10.54 ksi. Even this increase allows for a factor of safety to yield of 3.32, well over our goal of obtaining a FOS greater than or equal to 2.

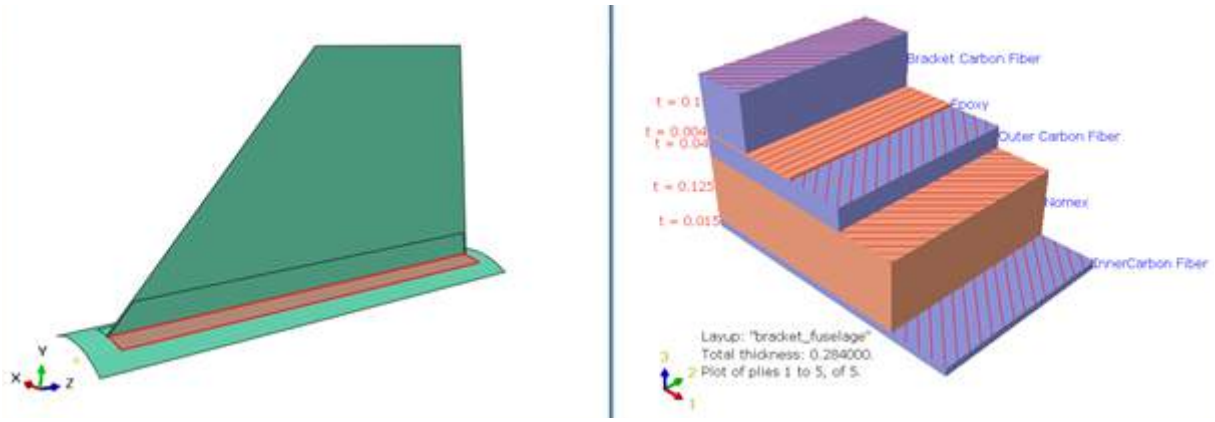

Figure C.3.8. LEFT: the location of the fin bracket including the fuselage. RIGHT: The layup stack plot, t = thickness in inches

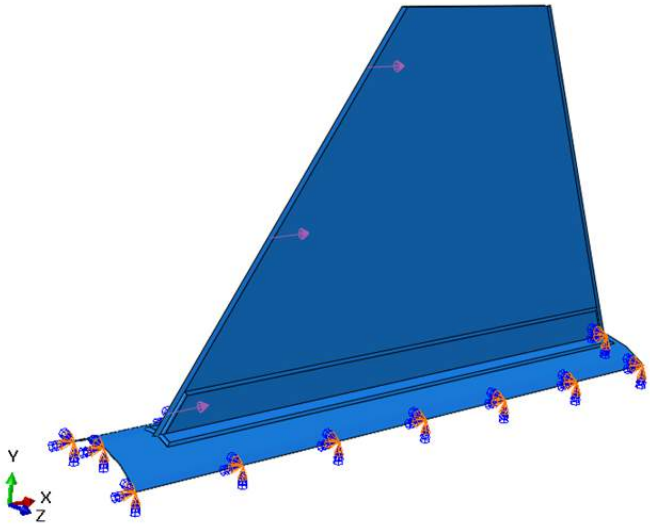

Figure C.3.9. The solid model of the fin assembly showing boundary conditions and area of load application.

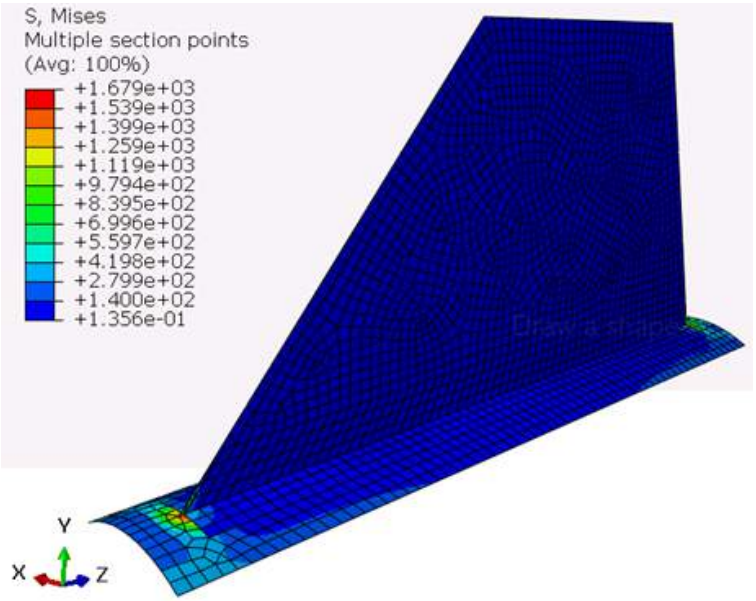

Figure C.3.10. The FEA results for the fin assembly shell model. Von Mises stress values in psi.

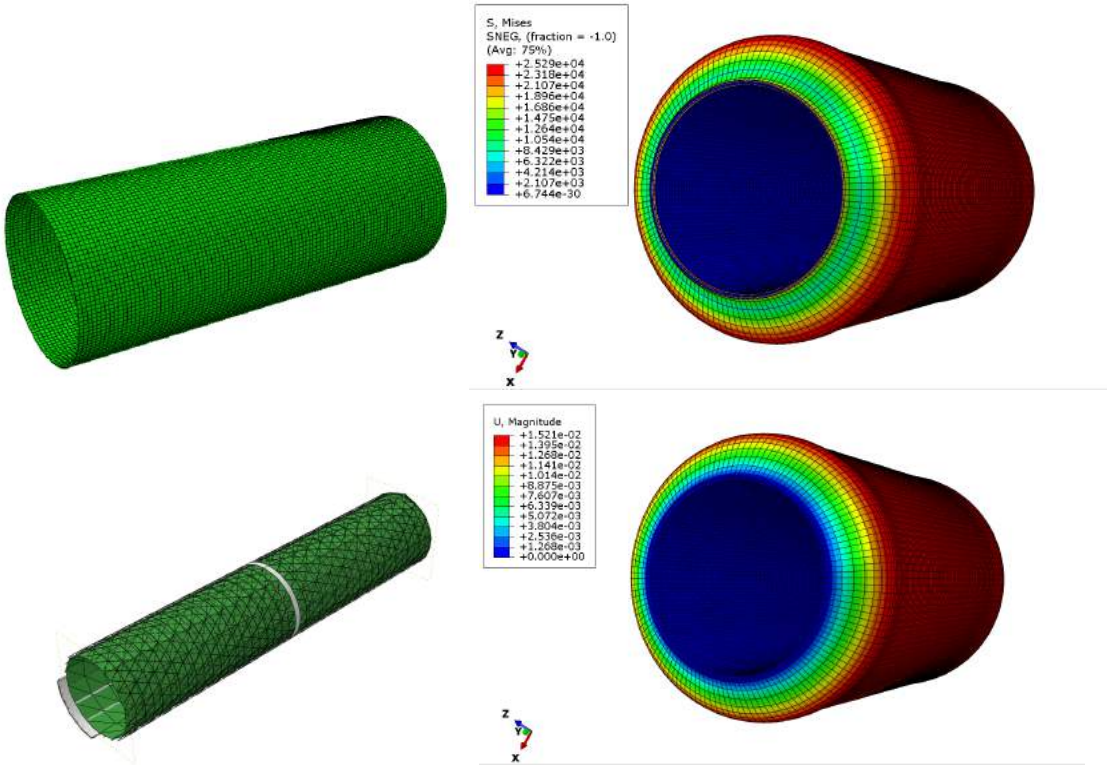

Figure C.3.11 LEFT: These simulations were modeled as equivalent thickness for the top and a partition of the entire isogrid CAD model in the two bottom. RIGHT: the results of the isotank simulation results that had very questionable deformation of 0.0152 inches even though max. Von Mises stress resulted in a FOS of 1.38.

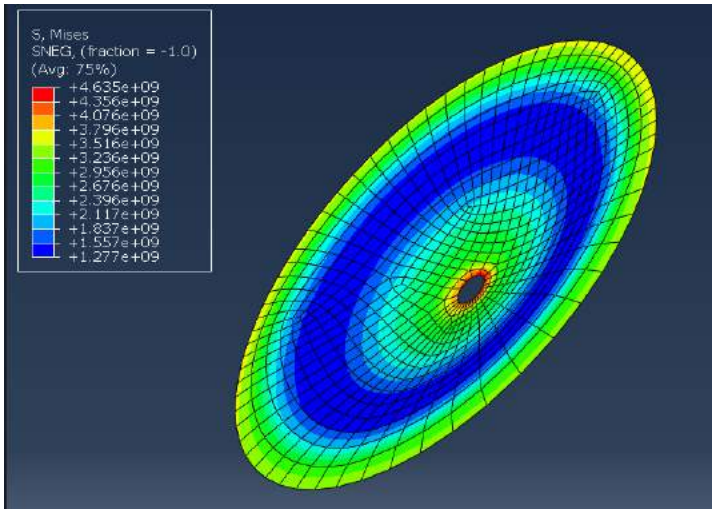

Figure C.3.12: End cap FEA on equivalent thickness with unrealistic results.

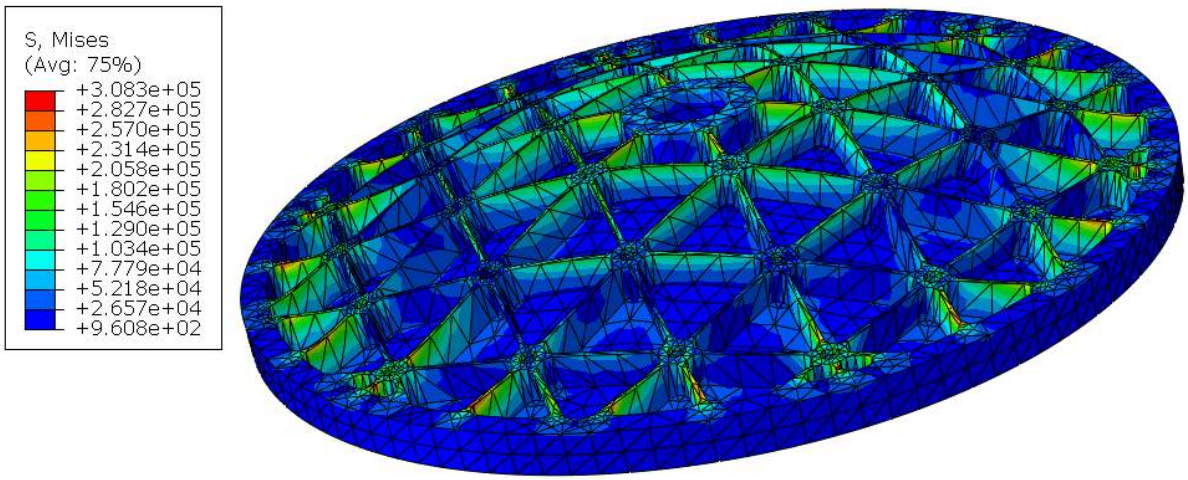

Figure C.3.13: End cap FEA on the imported geometry with better results but stresses still above the ultimate strength of aluminum.

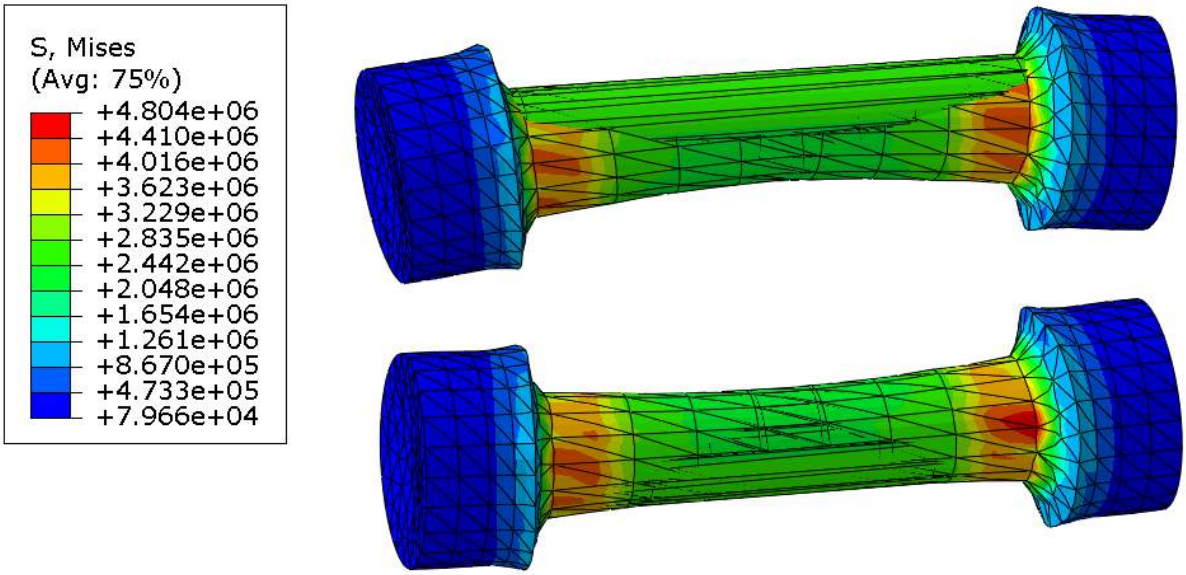

Figure C.3.14: FEA results from the Launch Lug Assembly simulation showing an excessive amount of stress delivered to the fasteners. This will be a key area of further evaluation for future teams

C.4: Training

Rockets are inherently complicated and dangerous, and the addition of a liquid fueled engine and reaction control system required an abundance of safety training.

a. International Traffic in Arms Regulations

The reaction control system of LV4 is used to control pitch and roll to stabilize the rocket during flight. This control system fits the US government criteria for a guided missile, thus falls within regulations of ITAR. ITAR is a governing body that prevents defense technologies from falling into the hands of foreign entities. Our future work may fall under ITAR restrictions so it was important to learn best practices for storing and sharing information to avoid fines or prison time.

b. Base11 Safety Training

The Base11 Space Challenge requires entrants to complete an approximately five hour long general rocketry safety program with a focus on liquid fueled rocket engine safety, and emphasis on best practices for designing fuel/oxidizer delivery systems.

c. NASA LOX Training

The NASA Technical Professional Training, Fire Hazards in Oxygen Systems program is an in-depth (approximately 15 hours long) instruction on liquid oxygen systems. While our team will not be directly working with any oxygen systems, they will play a major role in the LV4 project and the isotank design. This training taught us about the science of combustion reactions due to oxygen rich environments. It is important to have a fundamental understanding of this even in designing airframe components, since materials that are not flammable in air can be highly flammable in oxygen rich environments.

d. Isogrid General Design Metrics

An introduction to isogrid theory and manufacturing was given by our industry advisor, Peter McCloud. This training covered the history of the isogrid concept, reasons for use, current applications, and how the isogrid tanks will be made for LV4.

C.5: Risk Analysis

The team met with the PSAS Safety Officer to determine the likely modes of failure for the airframe and the risk these failures pose to the mission, the vehicle, the environment/property, and to people. Once risks were identified we used a Failure Modes and Effects Analysis (FMEA) to determine controls to implement in the design for mitigating risks. Figure C.5.1 shows effects of the most impactful event, a RUD upon boost, on people, the environment, the vehicle, and the mission. Figure C.5.2 shows the fault tree for this event with root causes identified and C.5.3 shows the root cause identification and likelihood assessment, with the rocket breaking in half being the most likely. Figure C.5.4 shows the current mitigation strategy and effectiveness assessment for controls of root causes of an RUD during boost, with an average risk reduction of 30%.

Event No.	FAF	Stage Impact	869	3. Boost					Updated: Updated by:	People present:
	Failure Event Description			Risk Domains: Persons	Environment	Vehicle	Mission	Impact	Impact Description	
3.1	R.U.D.			5	5	5	5	435	A rapid disassembly can cause serious personal or property damage and	
3.2	Disconnecting from launch rail improperly/too early			5	5	5	5	435	This can cause a unpredictable trajectory of the rocket.	
3.3								0		
3.4								0		
3.5								0		

Figure C.5.1: Impact and failure event identification for when the rocket is in its boost stage. Figure shows the two most impactful failure events: RUD and disconnecting from the launch rail improperly.

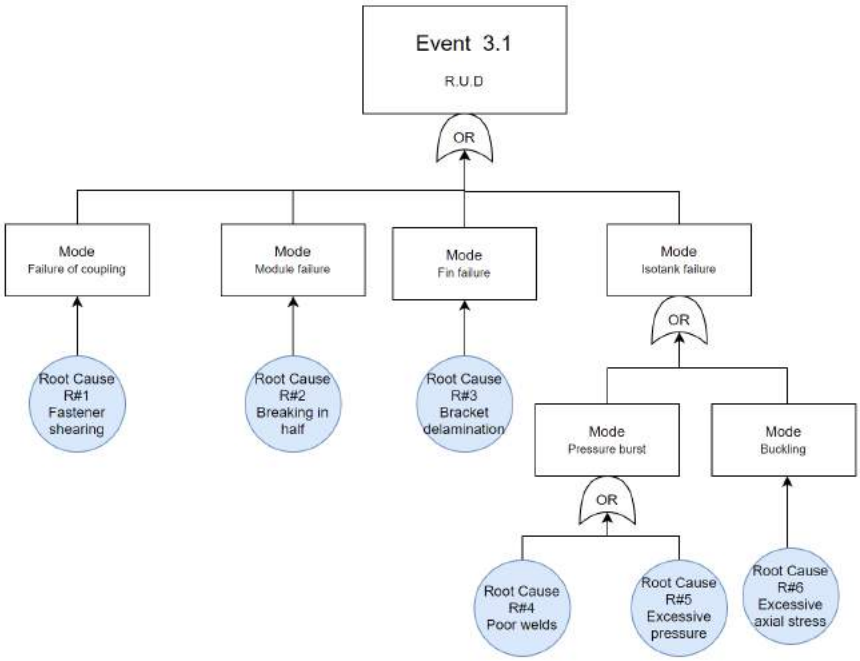

Figure C.5.2: Fault tree for RUD during boost with six root causes identified.

Failure Case 1

Event I.D.	Failure Event Description	Risk Domains					Impact Description
		Persons	Property/Env	Vehicle	Mission	Impact Score	
3.1	R.U.D.	5	5	5	5	435	A rapid disassembly can cause serious personal or property damage and result in mission failure
3. Boost		DO NOT EDIT IMPACT SCORES IN SPACES ABOVE! After linking cells, to edit impact scores return to the 'Impact & Failure Events Identification' sheet.					

Root Identification and Likelihood Scoring

	Root Id	Repeat/ Null	description	Domain	Result	Controls	Contblty	Est. Prob	Reasoning	Control Factor	Prob. Score	Likelihood	Root (RPN)
1	R#1	R	Fastener Shearing	ME	will cause parts to break apart	5	2	0.75%	Selecting fasteners can be controlled based on structural analysis results.	7	3	189	82122
2	R#2	R	Breaking in Half	ME	rocket will break	5	4	5%	Many factors cannot be accounted for in design	9	4	576	250277
3	R#3		Bracket Delamination	ME	fins will break off	5	4	1.5%	Difficult to simulate fin flutter and stresses on fi	9	4	576	250277
4	R#4	R	Poor Welds	ME	will cause tanks to break apart	5	2	0.5%	Correct welding process can help mitigate failure modes but it is difficult to replicate tested welds.	7	3	189	82122
5	R#5	R	Excessive Pressure	ME	tanks will explode	5	3	1.0%	This can be controlled by having pressure relea	8	4	512	222468
6	R#6		Excessive Axial Stress	ME	rocket will buckle	5	3	1%	Using FEA analysis, this failure mode can mitig	8	4	512	222468

Figure C.5.3: Root cause identification and likelihood assessment for RUD during boost. The rocket breaking in half is the most likely root cause.

Failure Case #	Date Initiated:	Last Updated:	Updated by:	Mitigation Effectiveness: Root Level Risk Reduction	Mitigation Effectiveness: Event Level Risk Reduction
1	2/10/2021	02/11/2021	Catie and Jim	-30.34%	-31.25%
Event ID	**Description**			Root RPN Reduced	Event RPN Reduced
3.1	R.U.D.			-336744	-69521
	Impacts				
	A rapid disassembly can cause serious personal or property damage and result in mission failure				

Mitigation Strategy

Design Description	Mitigation Effects
Rocket has been designed to withstand bending and buckling stresses.	The rocket has redesigned module couplings, increased fasteners sizing, and structural analysis is being performed on the rocket design.

These Auto generate with initial impact scoring. Only change due to implement mitigation strategy(s). A valid justification must be given for doing so.	Persons	Prop/Env	Vehicle	Mission	Impact	Impact change reasoning
	5	5	5	5	435	

Root Causes				Mitigation		Adjusted Root scoring								Mitigation Effectiveness		
Root Id	Repeat /Null	description	Domain	Mitigation Description	Strategy Type	Controls	Contblty	Est. Prob	Justification for score change	Mitigated	Control Factor	Prob Score	Likelihood	New Root (RPN)	Root RPN Reduction	Risk Reduction
R#1	R	Fastener Shearing	ME	Fasteners are sized correctly.		3	2	0.75%	Confident in fastener size.	x	5	3	135	58659	-23463	-28.57%
R#2	R	Breaking in Half	ME	Redesigned coupling rings		3	4	5%	Major design improvement.	x	7	4	448	194660	-55617	-22.22%
R#3		Bracket Delamination	ME	Careful epoxy layup		3	4	1.5%	Added strength.	x	7	4	448	194660	-55617	-22.22%
R#4	R	Poor Welds	ME	Welds performed by professio		2	2	0.5%	Confidence in welds	x	4	3	108	46927	-35195	-42.86%
R#5	R	Excessive Pressure	ME	Strong tanks		2	3	1.0%	Tanks design will have a factor of safety of 2	x	5	4	320	139043	-83426	-37.50%
R#6		Excessive Axial Stress	ME	Modules thickness is consider		2	3	1%	Modules are designed for expected loading	x	5	4	320	139043	-83426	-37.50%

Figure C.5.4: Current mitigation strategy and effectiveness assessment for RUD during boost with an average risk reduction of 30.

Appendix D: System-level Requirements Matrix

Figure D.1 shows the key customer requirements for this project.

	Scalable from LV3.1	Design for manufacturing	Design for assembly	Must be within scope of MDO	Fit in composite curing oven	Hold the dry mass on the launch rail	Hold maximum tank pressure of 285.25 psi	Stronger than the ultimate strength of carbon fiber and aluminum	Minimize aerodynamic drag	Reach 100 km	Withstand maximum dynamic pressure of 12.619 psi	Length to diameter ratio 27.1	Meets the dry mass of 242.6 lbs
Full assembly		X	X	X						X	X	X	X
Nosecone	X	X	X	X					X				
ERS	X	X	X	X									
RCS	X	X	X	X									
Cameras	X	X	X	X									
N2	X	X	X	X	X								
Avionics	X	X	X	X	X								
Isotanks		X	X	X			X	X					
End caps		X	X	X			X	X					
Passthroughs	X	X	X	X									
Fin Can	X	X	X	X	X				X				
Bulkheads	X	X	X	X				X					
Coupling Rings	X	X	X	X		X		X					
Arc Clamps	X	X	X	X		X		X					
Thrust plate	X	X	X	X				X					
Race Pipes		X	X	X									
Launch Lugs		X	X	X		X		X					

Figure D.1: System-level requirements matrix for LV4

Appendix E: Subsystem 1: Fins

1. Overview

The Portland State Aerospace Society (PSAS) is an amateur rocketry group working on a liquid fueled rocket that is intended to reach an altitude of 100 km. This rocket is known as Launch Vehicle 4 (LV4) and is shown in Fig. E.1. While the initial design for LV4 comes from scaling up the previous launch vehicle, LV3.1, many aspects of the design are untested and may need to change due to the demands of the higher speed and altitude. LV4 is currently 24 feet long with an outer diameter of 12 inches. The design is determined by the output of the LV4 Multidisciplinary Optimization (MDO) code [1], which is updated regularly with information such as component mass and engine thrust. For the V2 phase of the rocket, four different fin shapes were compared and the results of drag force and maximum pressure on the front of the fin were then used in FEA models to determine the likelihood of fin delamination. The V3 phase included refinement of the models and further analysis of the rocket traveling at maximum dynamic pressure. The diamond trapezoidal shaped fin was found to have the lowest drag force and lowest maximum pressure on the front surface. This shape of fin is also less likely to break upon landing compared to a swept fin.

Figure E.1: Version 3 (V3) of Portland State Aerospace Society's Launch Vehicle 4 (LV4) airframe.

1.1. Four Fin Shapes

The four fins under consideration have two planform shapes: trapezoid (Fig. E.2) and swept (Fig. E.3); and two cross-sectional shapes: rectangular and diamond (Fig. E.4). The diamond cross section is created by chamfering the front and back edges. The four shapes are abbreviated in this report as "RT," "DT," "RS," and "DS" as shown in Table E.1.

Table E.1: Table showing abbreviated names of the four fin shapes.

		Planform Shape	
		Trapezoid	**Swept**
Side Shape	**Rectangular**	RT	RS
	Diamond	DT	DS

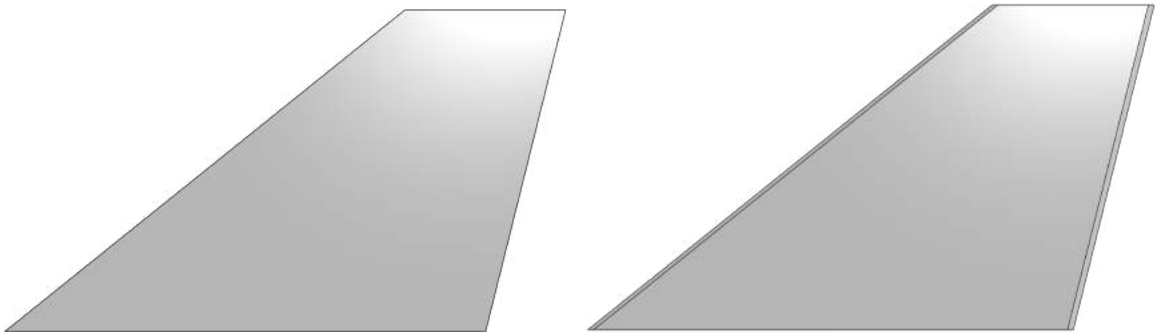

Figure E.2: Trapezoidal Fins. LEFT: Rectangular cross section (RT). RIGHT: Diamond cross section (DT).

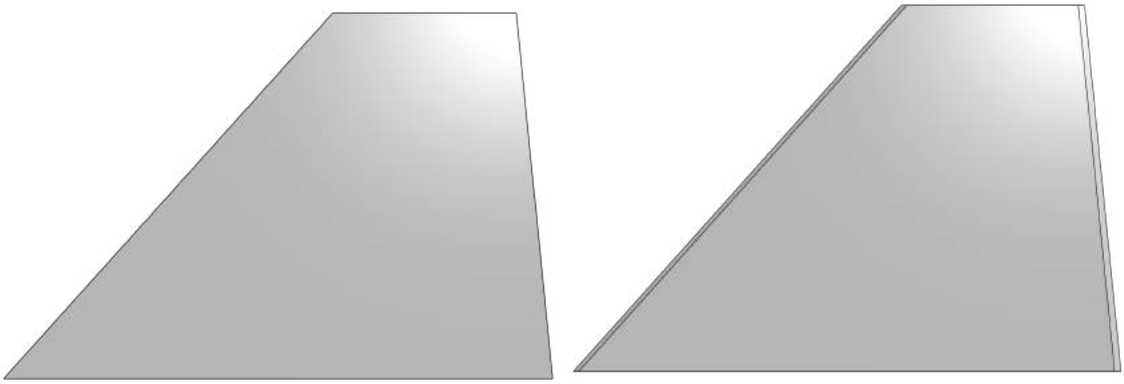

Figure E.3: Swept Fins. LEFT: Rectangular cross section (RS). RIGHT: Diamond cross section (DS).

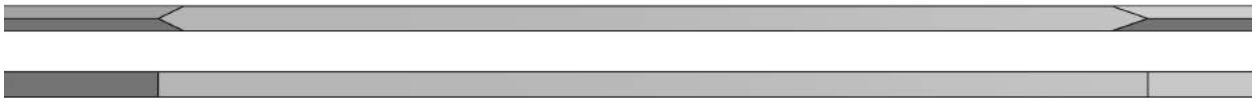

Figure E.4 TOP: Top view of a rectangular fin. BOTTOM: Top view of a diamond fin (front and back edges are chamfered).

1.2. Properties of Air and Flow at Altitude

This project uses an altitude of 9,993.3 m and a velocity of 617.29 m/s because the LV4 MDO is estimating a maximum dynamic pressure to occur at this instance. Table E.2 gives the values of the properties of the air flow field that will be used in this simulation:

Table E.2: *Properties of air flow field at an altitude of 9993.3 meters used in this simulation.*

Property	**Value**
Static Temperature	223.29 K
Density	0.356 kg/m^3
Dynamic Viscosity	1.4582 x 10^{-5} Pa-s
Absolute Pressure	22547.63 Pa
Thermal Conductivity	0.02035 W/m-K
Mach number	2.348
Velocity	617.29 m/s

2. Physical Model and Boundary Conditions

A simplified geometry of the body of the rocket with a nose cone was modeled to allow for the flow to develop before it reaches the fins. An overall rocket length of 24 feet was used with an outer diameter of 12 inches. Further detail of this geometry is not relevant to the flow at the fin surface. A trapezoidal fin was modeled at the end of the rocket using the geometry seen in Fig. E.5. Swept fins are created using a negative Offset Trailing value, while diamond cross sections are created by chamfering the edges after extrusion. The values used in the four simulations of this project are summarized in Table E.3, with all four fins having an equal planform area of 400 in^2, which is important for comparing drag and lift coefficients.

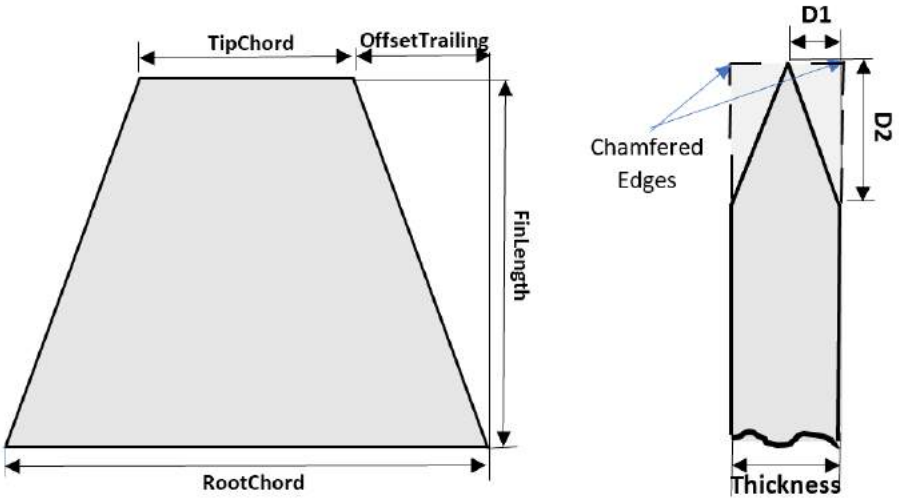

Figure E.5 LEFT: Planform view of geometry of a LV4 fin. Swept fins will have a negative Offset Trailing value. RIGHT: Cross section view of geometry of a diamond fin. D1 and D2 are dimensions of the chamfered front and back edges.

Table E.3: Table of values for fin geometry.

Variable	Description	Value [in]			
		RT	DT	RS	DS
RootChord	Length of bottom surface of fin	30	30	30	30
TipChord	Length of top surface of fin	13	13	13	13
OffsetTrailing	Distance from top back edge to bottom back edge	7	7	-7	-7
FinLength	Length from top surface to bottom surface of fin	16	16	16	16
Thickness	Thickness of fin	0.125	0.125	0.125	0.125
D1	Distance the chamfered edge is cut towards center line of fin	N/A	0.0625	N/A	0.0625
D2	Distance the chamfered edge is cut towards body of fin	N/A	0.56	N/A	0.56

The surrounding air flow was modeled as a cylinder with a rounded front surface and the entire geometry was cut to only ¼ of the full axisymmetric geometry, representing one of the four fins on the rocket (Fig. E.6). We can assume that the flow is axisymmetric about the rocket's centerline when there is no angle of attack to the flow (the rocket body, and thus the fins, are parallel to the flow). The values used in all four fin simulations are summarized in Table E.4.

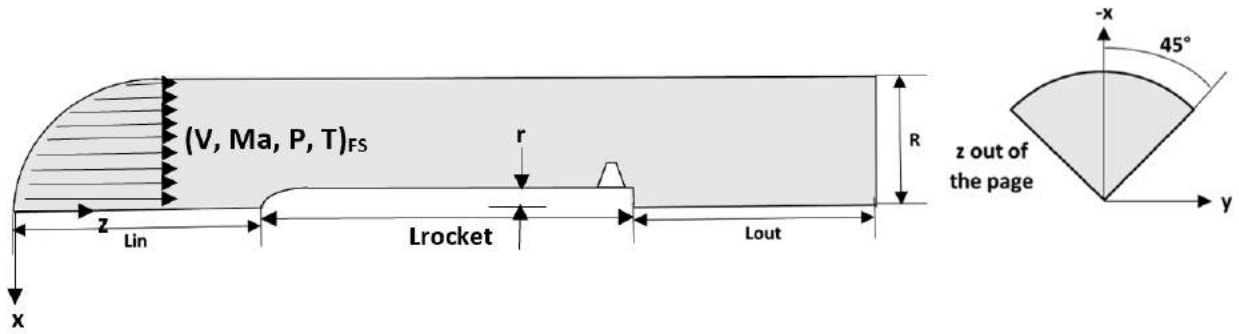

Figure E.6: Geometry of flow around rocket used in model.

Table E.4: Values of variables used in modeling CAD of flow geometry.

Variable	Description	Value [feet]
Lin	Distance from Free Stream start to rocket body tip	13
Lout	Distance from rocket body tail to Free Stream end	49
R	Radial distance of Free Stream cylindrical boundary	16.4
r	Radius of rocket body	0.5
Lrocket	Length of rocket body	24

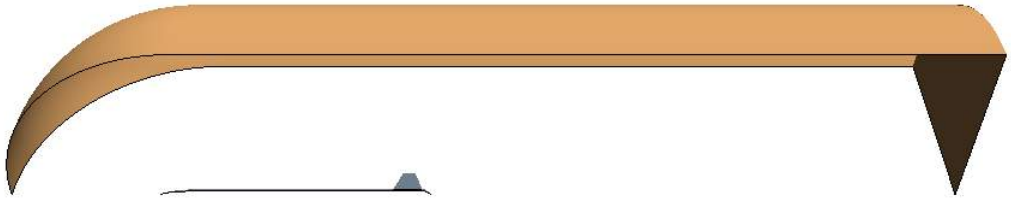

Figure E.7: The cylindrical surface is a boundary of type "Free Stream" and is shown in orange.

The cylindrical boundary surface seen in Fig. E.7 is of the type "Free Stream" [2]. Using the Mach Number + Pressure + Temperature option, the values from Table E.2 were used to change Flow Direction, Mach Number, Static Temperature, and Reference Pressure.

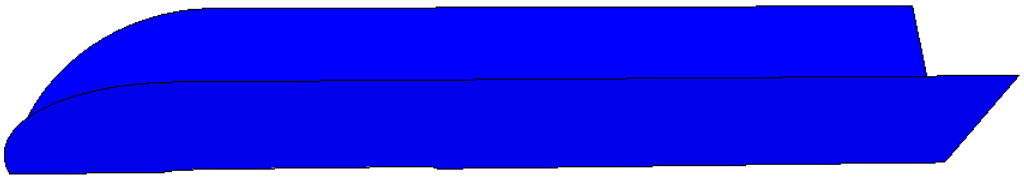

Figure E.8: The two surfaces resulting from the revolved cut of the axisymmetric geometry are shown in blue and are separate boundaries, each of the type "Symmetry."

The two surfaces that result from the revolved cut of the axisymmetric geometry are two separate boundary surfaces, each of the type "Symmetry" (Fig. E.8).

Figure E.9: TOP: Full rocket body. BOTTOM: The rocket body and fin surfaces are separate and of the boundary type "Wall."

The rocket body and fin are two separate boundary surfaces, each of the type "Wall," allowing for analysis to happen on the fin region alone (Fig. E.9).

3. CFD Software Features

The following models were selected for the Physics Continuum, with Auto-select turned on to result in all models shown in Fig. E.10:

- Two-dimensional
- Gas
- Coupled Flow
- Ideal Gas
- Steady
- Turbulent
- Spalart-Allmaras Turbulence [3]

The values for the Dynamic Viscosity and Thermal Conductivity of air were changed to match Table E.2, as well as the Reference Pressure, Initial Velocity, and Initial Static Temperature. The Minimum Allowable Pressure was changed to -1000 Pa to allow for negative pressures to develop behind the rocket.

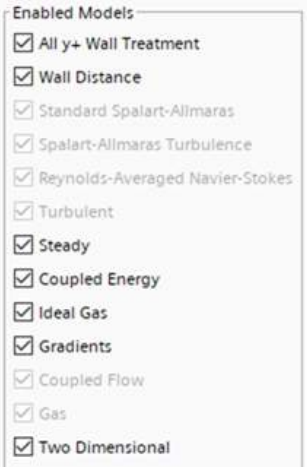

Figure E.10: Enabled Models for Physics Continuum.

4. CFD Mesh

The Automated Mesh used the following meshers: Surface Remesher, Trimmed Cell, Prism Layer. The modified values can be found in Table E.5, with all others left as default.

A custom surface control was used on the rocket fin and body with surface remeshing enabled and a Target Surface Size of 0.005 m.

Table E.5: Automated Mesh parameters that were changed.

Control	Value
Prism Layer Distribution Mode	Wall Thickness
Prism Layer Gap Fill Percentage	45.0
Prism Layer Minimum Thickness Percentage	0.05
Prism Layer Reduction Percentage	0.0
Base Size	0.1 m
Number of Prism Layers	10
Prism Layer Near Wall Thickness	0.015 m
Prism Layer Total Thickness	0.015 m
Maximum Size/Thickness Ratio	10.0
Maximum Cell Size	1.0 m

5. CFD Results and Discussion

Convergence was determined by plots of the coefficients of drag and lift on the fins. A line probe was created along the front surface of the fins. The pressure at each point along the line probe was plotted and the maximum value extracted. The drag force for each fin was also extracted and the results are shown in Table E.6. The diamond trapezoidal fin experiences the lowest drag force of 45.89 N and the lowest maximum pressure of 5.8 psi. These values were then passed along for use in FEA.

Table E.6: Summary of Drag Force and max frontal pressure for the four fin shapes at max dynamic pressure.

	FD (N)	P (psi)
RT	274.67	31
DT	45.89	5.8
RS	132.74	13.8
DS	93.05	6.05

6. FEA

The fins of Launch Vehicle 4 (LV4) are fastened to the rocket fuselage via a bonded bracket (Fig. E.11). Finite Element Analysis was performed with the Abaqus/CAE program to validate this method of fin attachment for LV4 using the following properties:

- CFD analysis of maximum pressure = 5.6 psi (38610.6 Pa)
- Epoxy tensile strength[4] = 5850 psi (4.0334e+7 Pa)

Material	Young's moduli
Carbon Fiber[5]	62 GPa
Nomex[6]	2.5 GPa
Epoxy[7]	3.81 GPa
Al 6061[8]	3.81 GPa

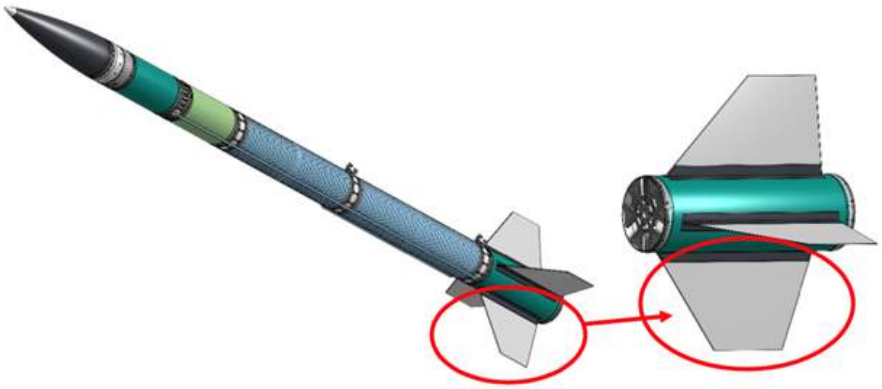

Figure E.11: LV4 with detail of bonded fin assembly.

6.1 Methods, shell model and solid model.

A shell model of a section of fuselage containing one fin is created dimensioned in inches. A mesh with Abaqus/CAE settings S4: A 4-node doubly curved general-purpose shell, finite membrane strains was selected with 2,474 elements. Encastre boundary conditions are used to represent the connection to the rest of the fuselage, as the area of interest for this study is the leading edge where the bracket is bonded to the fuselage. Drag forces of 5.6 psi are applied as a shell edge load to the leading edge of the fin. (Fig. E.12)

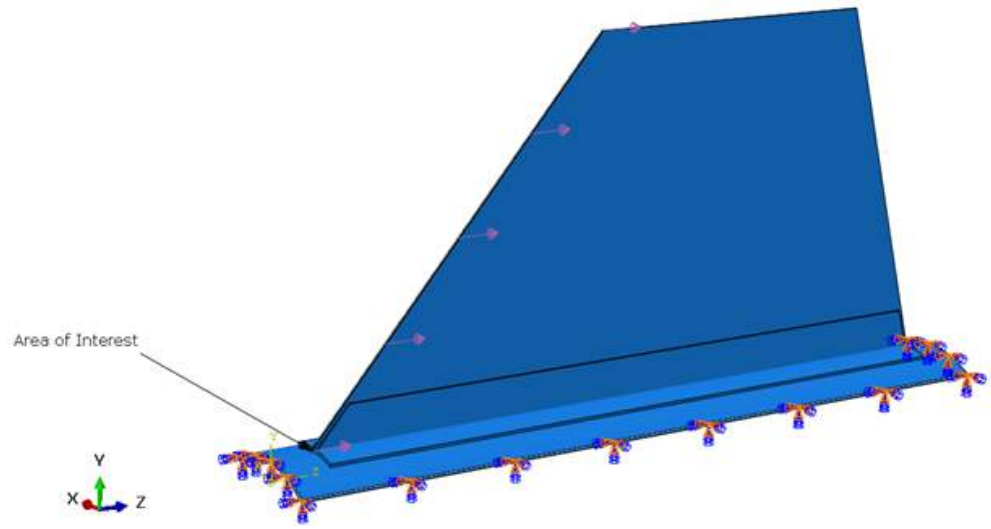

Figure E.12. The modeled fin assembly depicting location of load application and boundary conditions.

The reason the shell model was selected was because of the composite laminae feature, where the actual composite lay-up can be modeled. The figures below are visual representations of the ply stacks and their locations.

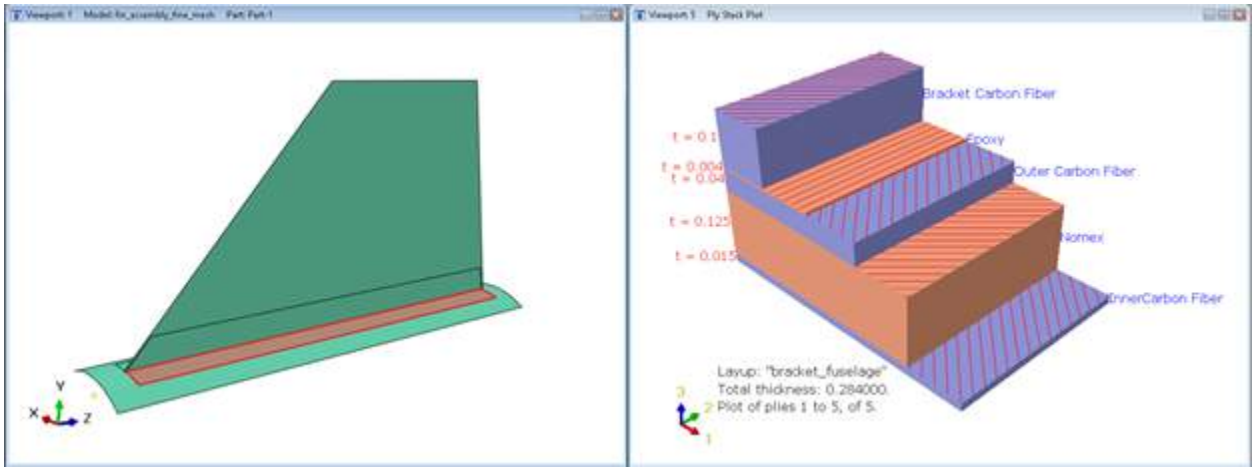

Figure E.13. The layup stack plot (right) and location (left) of the fin bracket including the fuselage, t = thickness in inches.

A solid model of the fin assembly was created to check the results from the shell model and to look for internal stresses that are not viewable in the shell model. The model was created by importing a CAD file of the assembly parts, as the default unit for CAD imports into Abaqus/CAE is meters, all inputs are converted to meter based SI units. The mesh with Abaqus/CAE settings C3D10: A 10-node quadratic tetrahedron was selected, with 18,019

elements. The model consists of a part containing the brackets and fin that are connected using a tie constraint to the fuselage (Fig. E.13). The fin and bracket part is partitioned for section assignment of carbon fiber and aluminum materials. As with the shell model, the encastre boundary conditions were applied. A pressure load of 38,610.6 Pa is applied to the leading edge of the fin (Fig. E.14).

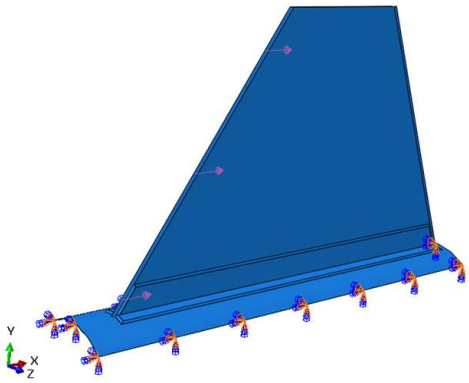

Figure E.14. The solid model of the fin assembly showing boundary conditions and area of load application.

6.3. Conclusion and discussion

The results of the shell and solid models were 1500.18 psi and 34.3 psi, respectively (Figs. E.15-E.18), which is less than the 5850 psi tensile strength of the epoxy that bonds the surfaces. However, the significant discrepancy between these two values indicated that one or both of these models is flawed. Ultimately, this is a study of the tensile forces that would peel the brackets from the fuselage. The construction of LV4 uses several layers of composite laminae, and the shell model uses inputs that model this in detail. However, the shell model is most accurate at modeling bending rather than tensile forces, and the solid model is better suited to tensile force analysis[9]. However, bonded joins are not necessarily going to react as in the real world using a tie constraint. More work needs to be done to accurately model the LV4 fin assembly.

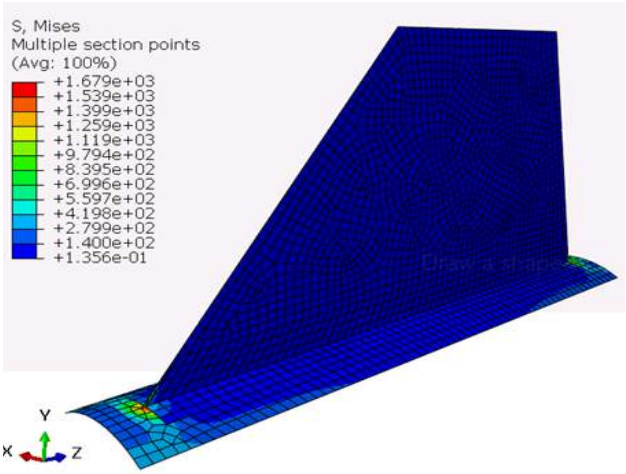

Figure E.15. The FEA results for the fin assembly shell model.

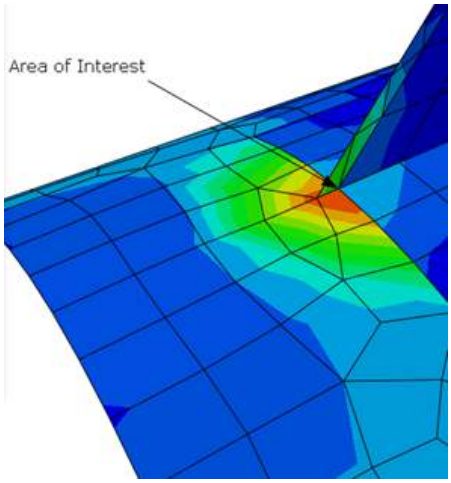

Figure E.16. The FEA results for the fin assembly shell model, enlarged with probe values at the elemental node at the area of interest.

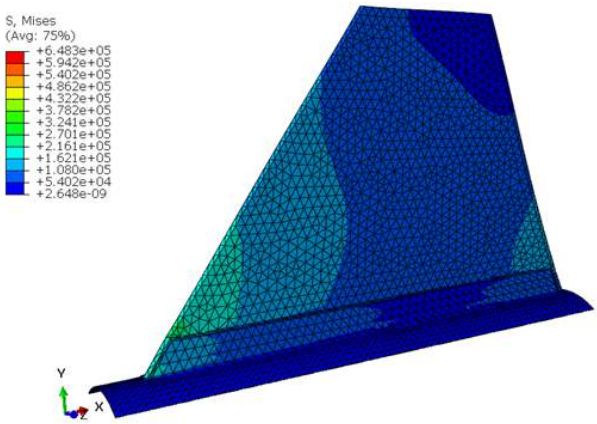

Figure E.17. The FEA results for the fin assembly solid model.

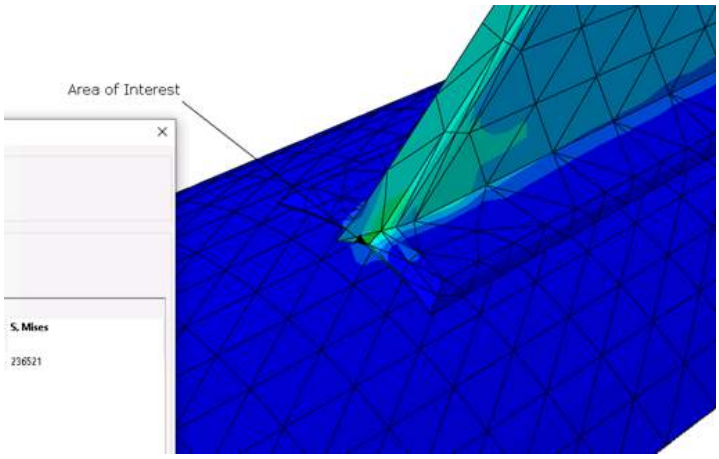

Figure E.18. The FEA results for the fin assembly solid model, enlarged with probe values at the elemental node at the area of interest.

7. References

[1] “LV4 MDO Simulation and Optimization,” Portland State Aerospace Society, retrieved February 2021. https://github.com/psas/lv4-mdo/tree/master/Simulation_and_Optimization

[2] Ewing, P., “Best Practices for Aerospace Aerodynamics,” *STAR South East Asian Conference*, Singapore, June 2015. http://mdx2.plm.automation.siemens.com/sites/default/files/Presentation/ExternalAero_SEA-ugm-2015.pdf

[3] “Transonic Flow: RAE2822 Airfoil,” STAR-CCM+ User Guide, Siemens, retrieved March 2021.

[4] Tzetzisa, D., Tsongasb, K., Mansou, G., “Determination of the Mechanical Properties of Epoxy Silica Nanocomposites through FEA Supported Evaluation of Ball Indentation Test Results”, Research Paper, School of Science and Engineering, International Hellenic University, Thermi,/Department of Mechanical Engineering, Aristotle University, Thessaloniki, Greece. http://www.scielo.br/scielo.php?script=sci_arttext&pid=S1516-14392017000601571&lng=en&tlng=en [Retrieved April 2021]

[5] Portland State Aerospace Society (PSAS) materials archive, CYCOM® 934 Standard Modulus 8 Harness Satin Fabric product data sheet.

[6] Chiang Foo, C., Boay Chai, G., Keey Seah, L., “Mechanical properties of Nomex Material and Nomex Honeycomb Structure”, Research Paper, Nanyang Technological University/School of Mechanical and Aerospace Engineering, Singapore https://www.researchgate.net/publication/222397543_Mechanical_Properties_of_Nomex_Material_and_Nomex_Honeycomb_Structure [Retrieved April 2021]

[7] Portland State Aerospace Society (PSAS) materials archive, ProGlas F-2400 1:1 Structural Adhesive product data sheet.

[8] Portland State Aerospace Society (PSAS) materials archive, “Aluminum Standards and Data 2006 Metric SI”, Aluminum Association Inc. product data sheet.

[9] Logan, D., “A First Course in the Finite Element Method”, Text Book, 6th Ed, Cengage, Boston Massachusetts, 2017.

Appendix F: Subsystem 2: Launch Lugs

The launch lugs hold the rocket on the launch rail horizontally during loading and then vertically during launch to provide initial guidance for the rocket trajectory. The six lug brackets contained in the three instances of launch lugs must carry the dry (unfueled) weight of the rocket estimated to be 242.6 lbs. by the MDO. The stress on the brackets must not exceed the ultimate strength of 6061-T6 aluminum (45 ksi). The fasteners holding the launch lug arc clamps to the coupling rings and the fastener pins holding the brackets in place must not shear.

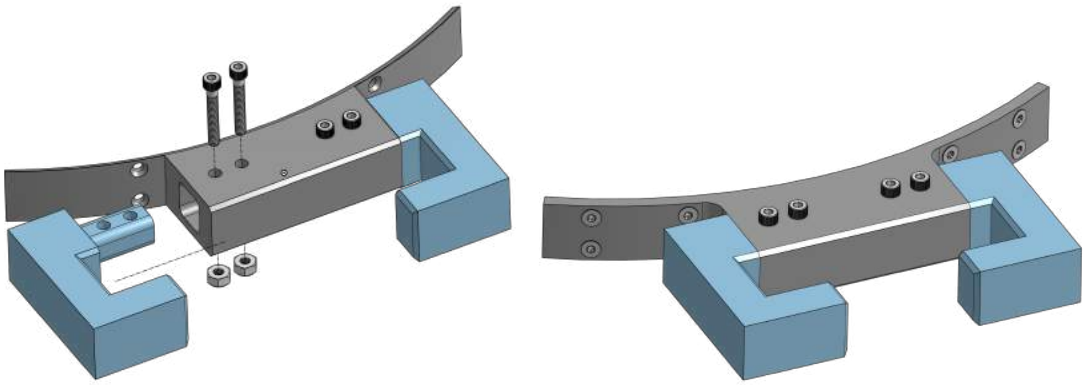

Figure F.1: Launch Lug assembly with brackets shown in blue.

The first requirement of these launch lug assemblies was to be able to hold the dry weight of the rocket horizontally. These specialized arc clamps fasten to the coupling rings of the rocket using 8 fasteners. The launch rail is clamped by the bracket portions which make up the blue "C" shape seen in Fig. F.1, holding the dry weight of the rocket as it is lifted by the launch rail from a horizontal, 0° position, to its launch position at 90° from horizontal. The horizontal hanging position just before it starts to slowly rise was determined to be the point of maximum static hanging weight and thus chosen as the analysis position for the worst case loading scenario.

Based on the rocket's loading sequence onto the launch rail, the six external launch lugs need to collectively support the entire hanging weight of the rocket. The total dry weight of LV4, unfueled, is 242.574 lbs. Dividing this weight of the rocket up between the six launch lug brackets, a convergence study was performed regarding the max Von Mises stress and max deformation obtained in the hanging of the rocket from these brackets. Loading was applied as a simple pressure load on the inside of the bracket flange as seen in Fig. F.3. The initial concern with the V1 and V2 versions was the stress concentration that is found in the 90° angle portion of the fastener hole area of Fig. F.2. The maximum stress values were 22.42 ksi in the 90° angle juncture and produced a factor of safety to yield of 1.56. This was too low of FOS value so a subsequent design approach utilizing a fillet in this region was performed.

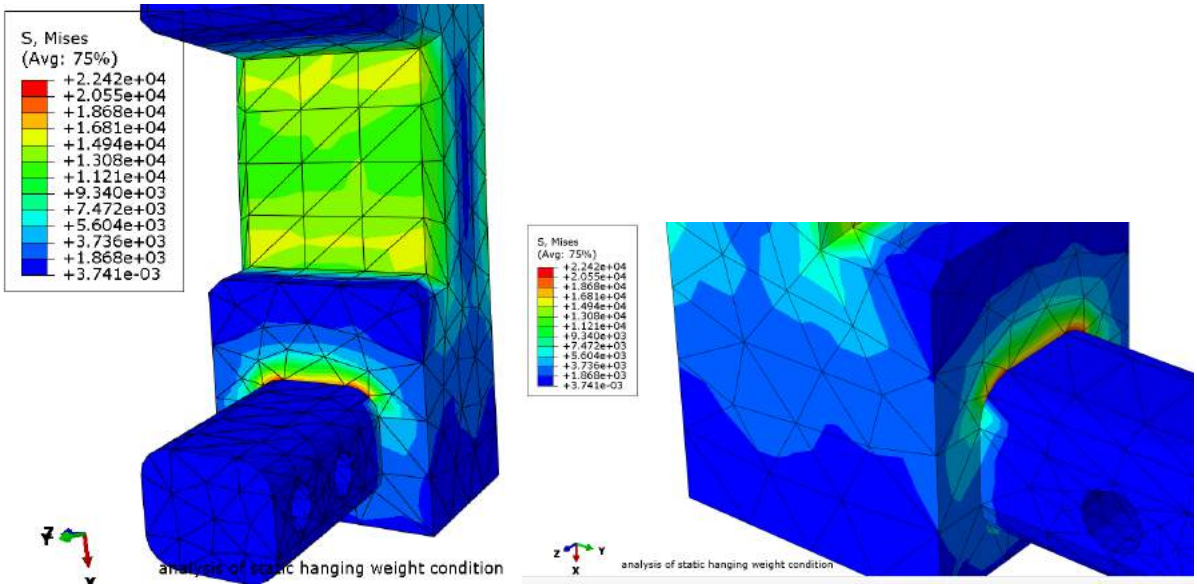

Fig. F.2: Visualization of the stress concentration that occurred in the first iteration of the launch lug bracket simulation.

After the fillet was added, a factor of safety to yield of 31.1-58.5 was determined, depending on the mesh number that is used. When using a large mesh number, the deformation converged while the maximum Von Mises continued to increase (Fig. F.3-F.5, Table F.1). This information will need to be further developed by future teams to see if a true convergence of the deformation and maximum Von Mises stress is possible by continuing to increase the mesh numbers.

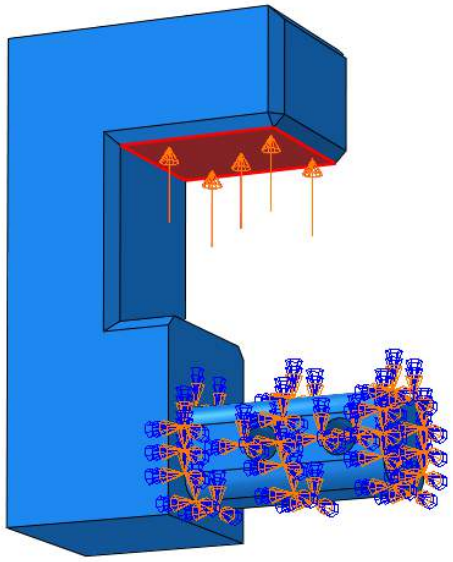

Fig. F.3 The Launch Lug bracket loading boundary conditions set up in Abaqus. Loading of 40.429 psi was applied to the inside of the bracket flange to mimic the dry weight of the rocket's mass distribution to one of the six launch lug brackets

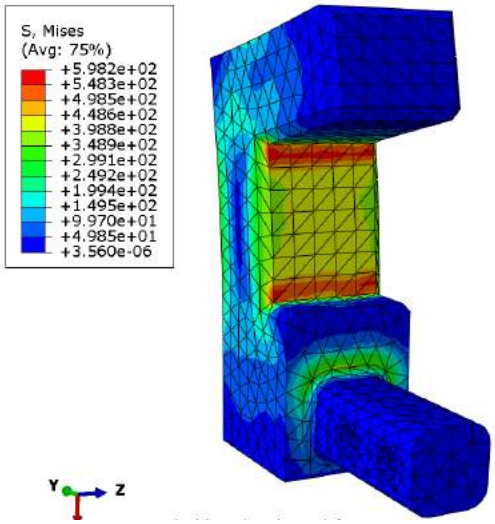

Mesh: 6891 mesh elements

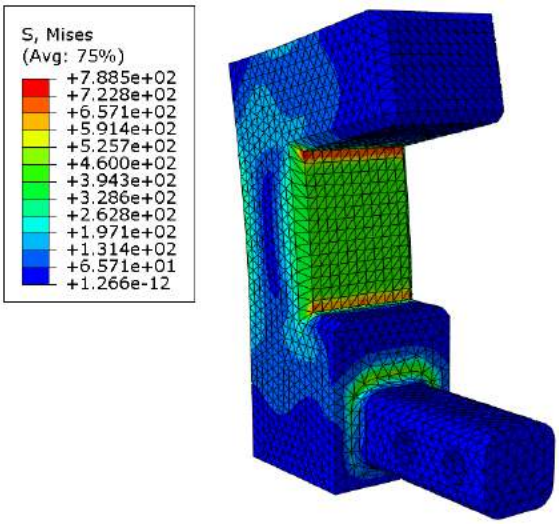

Mesh: 42,403 mesh elements

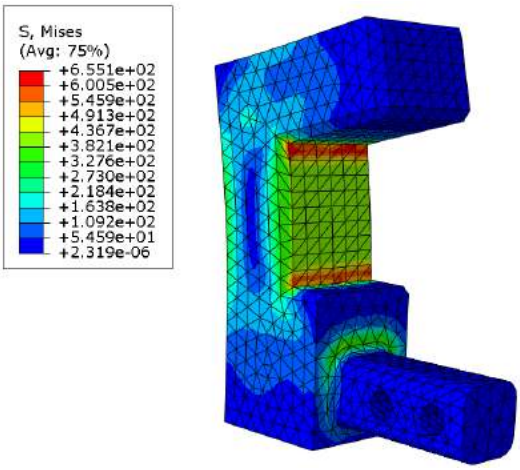

Mesh: 10,531 mesh elements

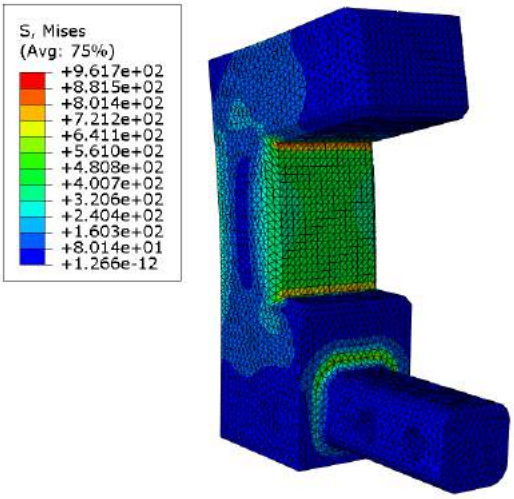

Mesh: 118,303 mesh elements

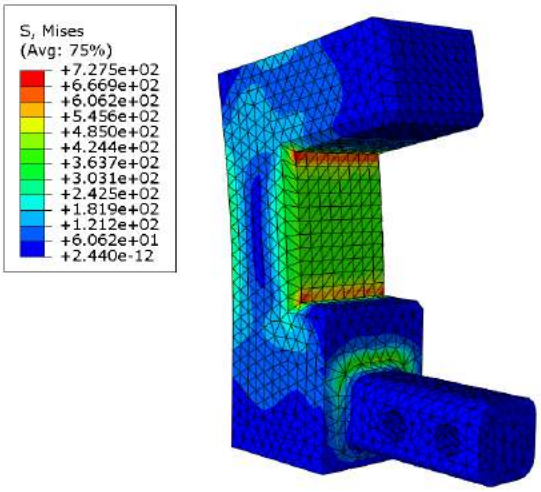

Mesh: 20,758 mesh elements

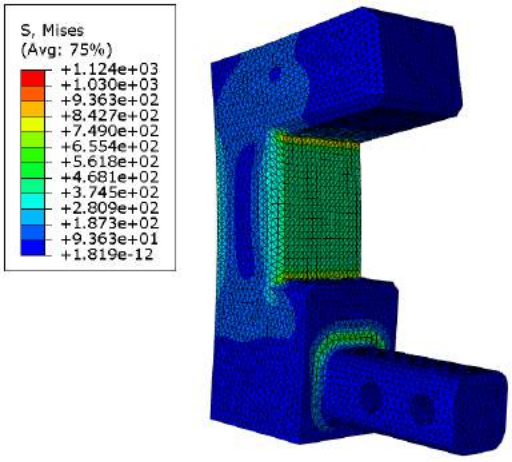

Mesh: 157,086 mesh elements

Fig. F.4: The series of six mesh refinements, continually increasing element number from top left to bottom left and then top right to bottom right, that were incorporated into the analysis of the launch lug brackets and the respective max. Von Mises stress.

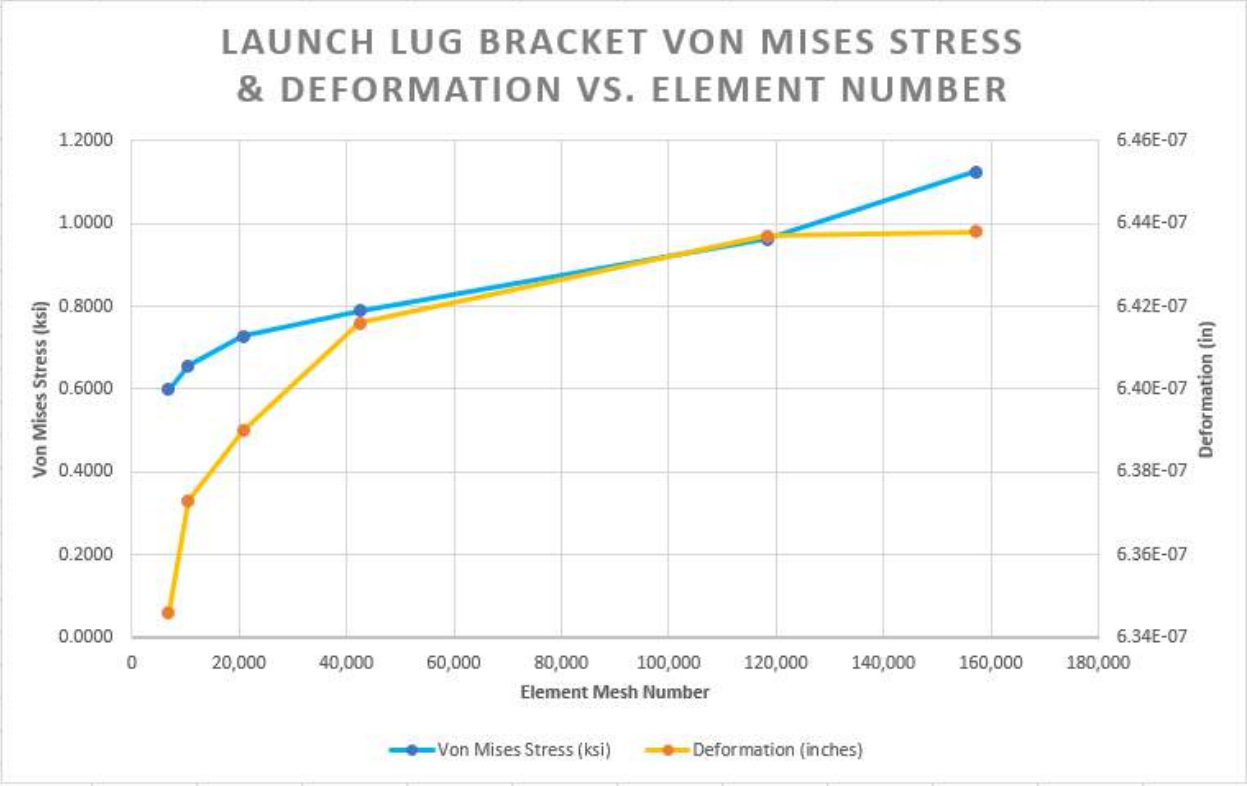

Fig. 5: Convergence study for the Launch lug bracket comparing the onset of maximum deformation as related to the refinement of mesh grid and maximum von Mises stress

Table F.1: Data pulled from Abaqus simulation of the Launch Lug Brackets detailing the number of elements in the mesh grids and their respective deformation and Von Mises stress outputs.

Mesh Elements	Von Mises Stress (ksi)	Deformation (inches)
6,891	0.5982	6.35E-07
10,531	0.6551	6.37E-07
20,758	0.7275	6.39E-07
42,403	0.7885	6.42E-07
118,303	0.9617	6.44E-07
157,086	1.124	6.44E-07

Appendix G: Subsystem 3: Isotanks and End Caps

The isogrid tanks (Figure G.1) are a new technology for PSAS and were not implemented in LV3.1. They needed to be designed for a maximum tank pressure of 285.25 psi and hold under the ultimate strength of 6061-T6 aluminum (45 ksi). The tanks had to be able to be machined using a 4-axis CNC (Figure G.2). Each tank had to be made in two pieces and welded together in the center due to the length limitation of the CNC.

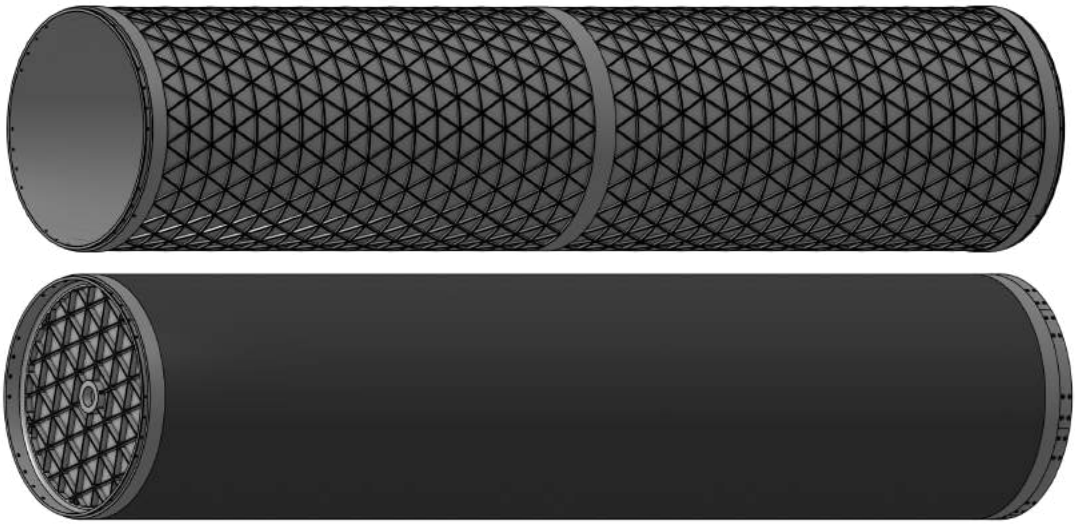

Figure G.1: TOP: An isogrid tank showing the isogrid pattern as well as the center weld margin where the two halves are joined. BOTTOM: an isogrid tank subassemblies with end caps and an aeroshell covering the isogrid pattern.

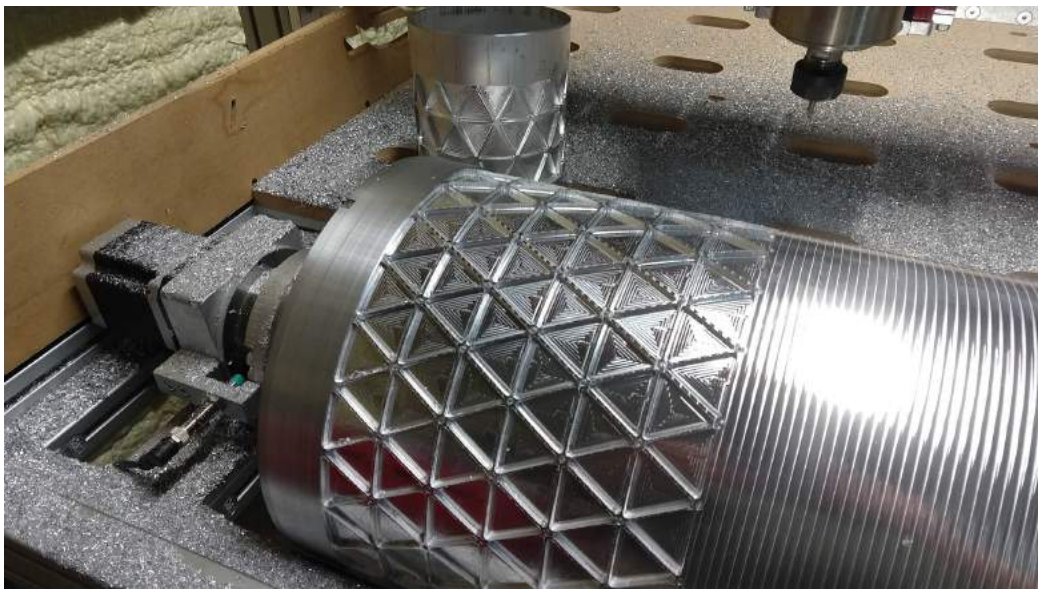

Figure G.2: The first isogrid tank in progress being machined on a 4-axis CNC by Peter McCloud.

Two main areas of concern were approached for understanding failure mechanisms of the isogrid tanks. First was the mechanical failure modes of the machined isogrid tanks themselves while the

second was the weld seams that would be present where the two tanks become secured together and where the end caps secure to each tank.

One loading scenario was approached as justification for not using flat metal sheeting with the isogrid machined into it and then rolled into a tube, as many large scale rocket manufacturers do for their isogrid tanks. The weld seam that holds the two ends of the sheet experienced very high levels of stress, further proving the manufacturing approach of milling a solid tube. As shown in Fig. G.3, the stress concentration surrounding the weld seam reached stress levels exceeding the ultimate tensile strength, outlining imminent failure.

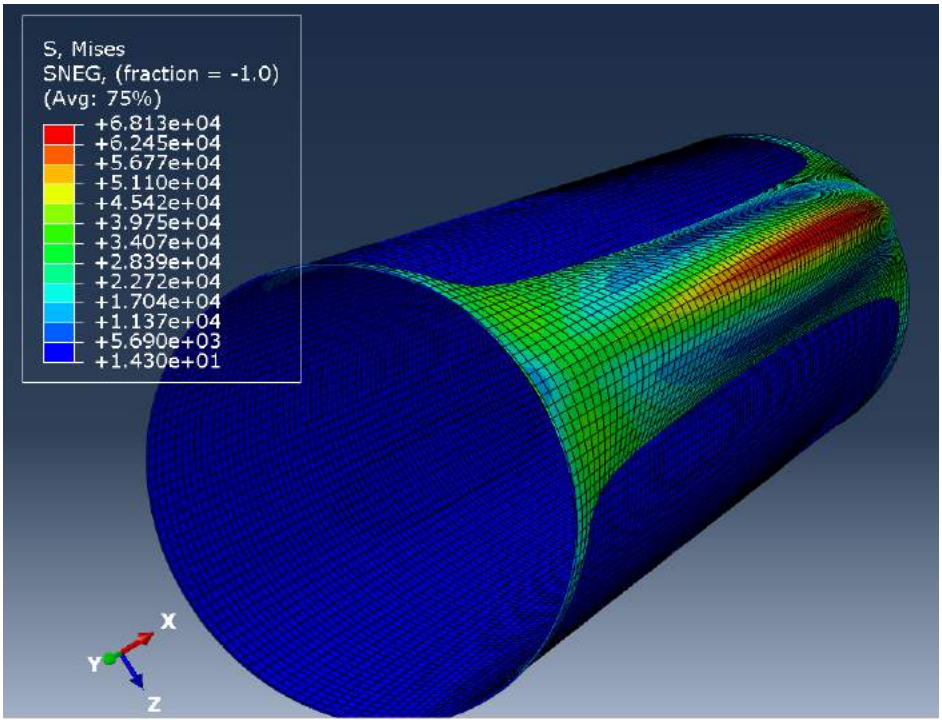

Fig. G.3: Welding seam analysis for the isotank mimicking the flat metal sheet rolled into a tube.

The isogrid end caps are a subsystem of the isogrid tank that is welded to the ends of the isotank, sealing the tanks that will contain the fuel and oxidizer for LV4. The end caps are machined with an isogrid pattern similar to the tanks they are welded into (Figure G.1). A hemispherical end cap is a more ideal shape for a pressure vessel end cap, but due to the complexity and added cost of manufacturing and welding a hemispherical shaped end cap with friction-stir welding, the flat end cap design was chosen. The flat end cap is subject to stress concentrations under pressure, so the end cap was the focus of FEA to determine the ideal balance of strength and weight (Fig. G.4 and G.5).

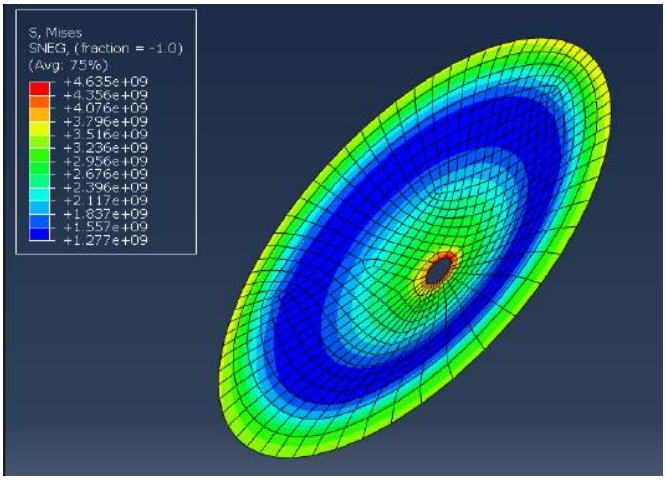

Fig. G.4: A model of the end cap in Abaqus utilizing a flat plate modeling approach that mirrors the boundary conditions and mechanical properties used are of an end cap that is TIG welded onto the iso tank. Results ended up giving us stress values over eight magnitudes too large in value.

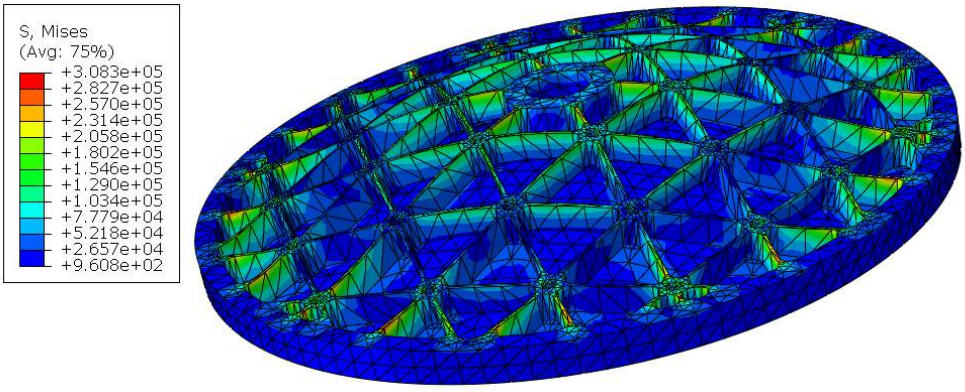

Fig. G.5: Analysis of the actual end cap solid model for comparison to the flat plate model seen in Fig. G.4. Although not quite as inflated stress values were found in this approach, the results still far exceed any tolerable levels of Von Mises stress

Operating internal pressure outlined by the MDO optimization was set at 245 psi which has been seen to cause permanent deformation in the below models of solid cylinder tanks. The goal to maintain a factor of safety of at least 2 requires maximum stress levels occurring in these simulations to be less than 22.5 ksi for the isotanks. Current simulations in Abaqus using the full cylinder extrude approach put the resulting maximum Von Mises stress for the tank at 50.46 ksi. It should be noted that the equivalent thickness approach was used in the creation of these models while the regular Young's Modulus was set as the mechanical properties of the 6061-T6 per normal approach. The validity of this approach should be double checked in future work to verify if another value for an alternative equivalent Young's Modulus value needs to be used instead. These results were obtained from applying an internal pressure of 245 psi, applying a thrust load of 5400 lb and also a 1400 lb drag load, similarly obtained by the MDO. The outputs from this series of simulations further suggests that the tanks are operating at too high of an internal pressure. Fig. G.6 shows an approach to find a suitable tolerable internal pressure by lowering the internal pressure attributed to the isotank's interior surface until a maximum Von

Mises stress was arrived at, with reassuring results within the factor of safety goal guidelines. Using the same mesh element number for two separate iterations, the factor of safety of 2 was finally obtained by lowering the internal pressure load to 80 psi. The resulting max stress fell from 50.46 ksi to 16.50 ksi for the 1,170 element mesh and from 56.70 ksi to 18.51 ksi for the 13,467 mesh element models.

Subsequent iterations of the isotank modelling were approached to try to alleviate the strange deformation values and visualization of the ends of the tanks. This was accomplished only by introducing inaccurate boundary conditions which did not reflect the physical restraints of the modules. A strong emphasis will be placed on subsequent future work and focus for these isotank and end cap simulations.

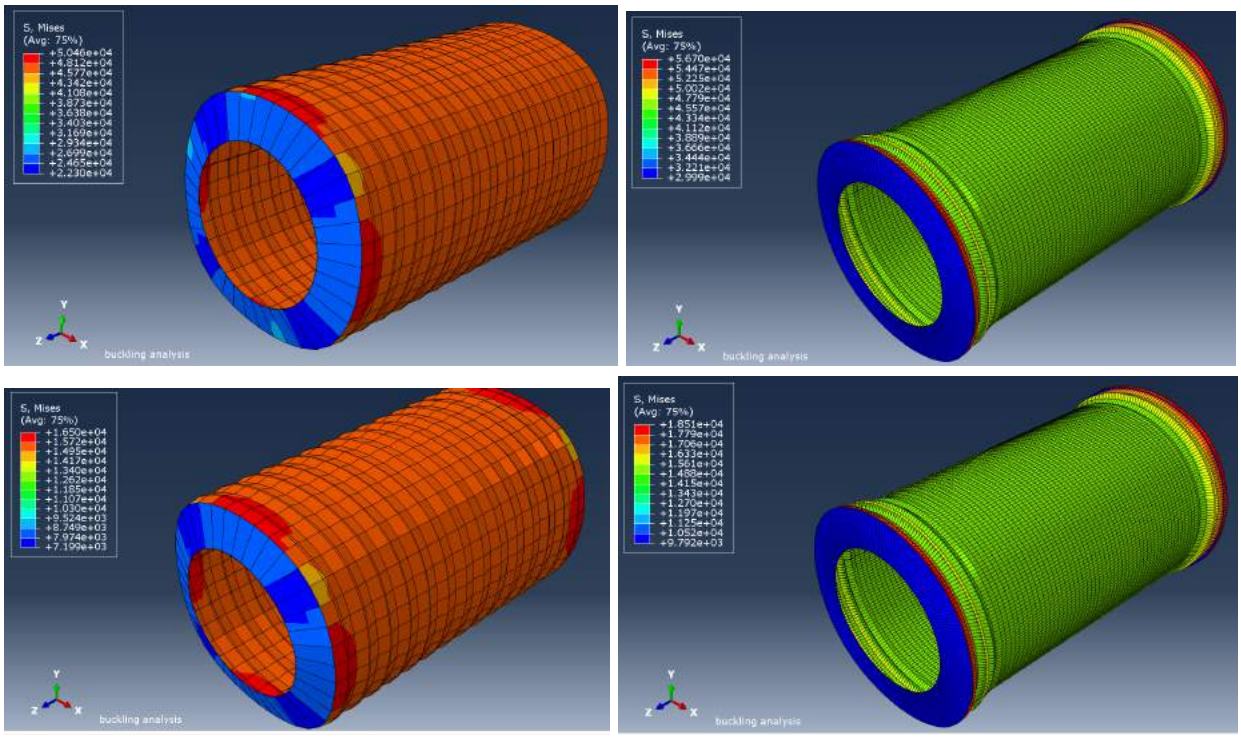

Fig G.6: Representations of the different sized mesh grids and resulting Von Mises stress. TOP LEFT: the mesh grid size of 1,170 elements, internal pressure of 245 psi, and max compressive loading scenario with a max. Von Mises stress of 50.46 ksi. TOP RIGHT: increased mesh element model of 13,467 elements under the same pressure and compressive loading with a max. Von Mises stress of 56.70 ksi. BOTTOM: the downgraded internal pressure of 80 psi gave acceptable results with the same meshes from the above two photos, respectively.

Appendix Z: ABET Objectives

Z.1: ABET Learning Outcome 1

1. *Case 1: Fins*

The fin assembly of the LV4 rocket is a scaled up version from LV3.1 which uses bonded carbon fiber brackets to attach the fins. Given the increased speeds of LV4, it was important to determine if the fin brackets would delaminate as a result of drag forces. Computational Fluid Dynamics simulations were done on the rocket using four different fin shapes using the properties of flow when the rocket is to experience maximum dynamic pressure. The drag force and maximum frontal pressure of the fins was extracted and used in Finite Element Analysis. The diamond trapezoid fin was found to have the lowest drag force and pressure (see Appendix C.2 and E). Two FEA models were created, a shell model of composite laminae and a solid model. The shell model was used to take advantage of the composite laminae feature, in which every layer of the composite is modelled with individual mechanical properties, including the epoxy used to bond the brackets to the fuselage. The solid model was created from imported CAD files, this was done to represent the precise geometry of the fin assembly and to investigate internal stresses that are not viewable in a shell model. The diamond trapezoid fin shape was found to be sufficient, with no delamination occurring.

2. *Case 2: Nose Cone*

The shape of LV3.1's nose cone was determined to be parameterized as an equation driven curve in the CAD, which was scaled up for LV4. Research into nose cone shapes, known as ogives, showed that the equation used was a form of the Von Karman ogive, which is designed to reduce drag. This is further parameterized by the fineness ratio which is the length to diameter ratio. A 5:1 fineness ratio is considered to be the best ratio for minimizing the effects of drag. To study the drag effects of the nose cone, simulations were run in a CFD simulation program, Star CCM+, to compare a fineness ratio of 3.6:1 (base case) and 5:1 (Appendix C.2). To set up the study of the nose cones in Star CCM+, implementation of the correct solvers, boundary conditions, stopping criteria, and initial values had to be correctly set up in the simulation. To understand the functions of these parameters and the effects of flow in a supersonic regime required understanding of applied and computational fluid dynamics. The main outputs of interest for this project were drag (pressure and skin) and the drag coefficient. Results from the base case were a drag force of 290.6 N and a drag coefficient of 0.042.

3. *Case 3 - Arc clamp Confirmation Analysis*

The arc clamp and coupling ring system of LV3.1 created a bending moment which ultimately caused the fastener bolts to shear, resulting in rocket failure. The redesign had to eliminate this unintentional moment to negate any future bending inflicted upon the fasteners of LV4 and instead cause the moment to be taken up by the arc clamps in the form of a tensile or compressive load to the bolts. This design was verified by delivering various moment load scenarios in Abaqus FEA and examining the resulting stresses on them. The simulation results showed a maximum Von Mises stress of 5.860 ksi occuring in the fasteners (Appendix C.3). The associated factor of safety to yield was 5.97. The applied loading was sourced from the mathematical relationships outlined in the MDO and the worst case scenario was found to be during the dynamic shift from compressive to tensile loading at burnoff.

Z.2: ABET Learning Outcome 7 - Isotank Design

In order to minimize mass, the sponsor decided to use isogrid tanks in LV4 to hold the Isopropyl Alcohol and Liquid Oxygen (see Section 3). This isogrid design ultimately allows for a material, in this case a thin walled pressure vessel, to be analyzed as having isotropic properties while minimizing mass. The team had minimal prior exposure to isogrid design and theory. The areas of concern were the design approach behind the isogrid, the supporting math detailing the load distributions, defining variables/non dimensional variables for modes of failure definitions, and the manufacturing constraints that the team would have to either work around or find solutions to. These requirements meant that the team needed to understand how these isogrid structures experienced applied loading and then apply these lessons to the main modes of failure that LV4 was likely to experience during flight. Inherent to the Isogrid design is its high strength-to-weight ratio, isotropic properties, and its redistribution of loads should any failure occur.

Peter McCloud, a PSAS faculty advisor, delivered an "Isogrid Primer" lecture on the various lessons and takeaways from the Nasa Isogrid Design Handbook [1]. This lecture detailed the mathematical theories behind isogrid designs as well as the CAD and manufacturing requirements. Previous CAD models had been done incorrectly and would have resulted in manufacturing difficulties and errors upon export to CAM. Additional research and work was done in correcting the CAD and ultimately producing separate CAM for manufacturing. FEA was also required to verify the theoretical stress values prior to manufacturing.

Although the concepts outlined in the NASA Handbook utilize an I-beam shaped flange that is undercut into each rib, due to the manufacturing constraints the rib design will resemble straight walled ribs. Initially designed in Onshape, the isogrid tanks were moved to SolidWorks due to the computation needed in creating the isogrid pattern. When completing FEA, an equivalent thickness along with an equivalent Young's modulus is used to enable the simulation to only utilize an isotropic cylindrical model without having to incorporate any of the computationally heavy isogrid design detail. The team met with Dr. Hormoz Zareh of Portland State University, who teaches FEA, to discuss modeling techniques for the tanks. Ultimately the current simulations in Abaqus can not verify the strength of these equivalent thickness models for neither the endcap nor the tank bodies. While the tank analyses did show the maximum Von Mises stress is not of concern, the deformation they incurred during the simulation raised some red flags. Additionally, the end caps, the most failure prone piece of these modules, showed excessive failure past the ultimate tensile strength. This was discussed with McCloud who then revisited the numerical calculations for the end caps and concluded that the thickness should be increased.

References

[1] "NASA CR-124075 REVISION A - ISOGRID DESIGN HANDBOOK." *Https://Www.nasa.gov/Goddard*, MCDONNELL DOUGLAS ASTRONAUFILS COMPANY, Feb. 1973, femci.gsfc.nasa.gov/isogrid/NASA-CR-124075_Isogrid_Design.pdf.